scientific reports

Check for updates

OPEN

Experimental and theoretical studies on induced ferromagnetism of new (1 – *x*) $Na_{0.5}Bi_{0.5}TiO_3$ + *x*$BaFeO_{3-\delta}$ solid solution

Dang Duc Dung[1]✉, Nguyen Huu Lam[1], Anh Duc Nguyen[1,2], Nguyen Ngoc Trung[1], Nguyen Van Duc[3]✉, Nguyen The Hung[1], Yong Soo Kim[2]✉ & Dorj Odkhuu[4]✉

New solid solution of $Na_{0.5}Bi_{0.5}TiO_3$ with $BaFeO_{3-\delta}$ materials were fabricated by sol–gel method. Analysis of X-ray diffraction patterns indicated that $BaFeO_{3-\delta}$ materials existed as a well solid solution and resulted in distortion the structure of host $Na_{0.5}Bi_{0.5}TiO_3$ materials. The randomly incorporated Fe and Ba cations in the host $Na_{0.5}Bi_{0.5}TiO_3$ crystal decreased the optical band gap from 3.11 to 2.48 eV, and induced the room-temperature ferromagnetism. Our density-functional theory calculations further suggested that both Ba for Bi/Na-site and Fe dopant, regardless of the substitutional sites, in $Na_{0.5}Bi_{0.5}TiO_3$ lead to the induced magnetism, which is illustrated in terms of the exchange splitting between spin subbands through the crystal field theory and Jahn–Teller distortion effects. Our work proposes a simple method for fabricating lead-free ferroelectric materials with ferromagnetism property for multifunctional applications in smart electronic devices.

The current research trend in materials science is injecting ferromagnetism into ferroelectric materials to create next-generation smart electronic devices[1,2]. The development of ferromagnetism materials based on lead-based ferroelectric by doing transition metals, such as $PbTiO_3$, has been hampered because their materials strong adverse effect on the environment and human health[3]. Ferroelectric lead-based $PbTiO_3$ materials are more commonly used than lead-free ferroelectric materials, such as those based on $Bi_{0.5}(Na,K)_{0.5}TiO_3$, $(K,Na)NbO_3$, or $(Ba,Ca)(Zr,Ti)O_3$[4,5]. $Na_{0.5}Bi_{0.5}TiO_3$ as one of common lead-free ferroelectric compounds has been considered as a promising candidate that can be replacement for lead-based substances because of its stronger polarization[3]. The high polarization of $Na_{0.5}Bi_{0.5}TiO_3$ materials is due to the lone pair effect of Bi^{3+} in comparison with that of Pb^{2+} in perovskite structures[6,7]. Therefore, injecting room-temperature ferromagnetism into lead-free ferroelectric $Na_{0.5}Bi_{0.5}TiO_3$ is one of significant research interests.

Scholars have developed $Na_{0.5}Bi_{0.5}TiO_3$-based materials with room-temperature ferromagnetism property by using transition metals, such as Co, Fe, Mn, or Cr[8–11]. Moreover, the solid solutions of $Na_{0.5}Bi_{0.5}TiO_3$-based materials with $BiFeO_3$ material exhibits room-temperature ferromagnetism[12]. $Na_{0.5}Bi_{0.5}TiO_3$ materials are composed of ferrite compounds, such as $CoMn_{0.2}Fe_{1.8}O_4$[13]. Ju et al. predicted that substituting a transition metal cation to Ti-site results in the magnetic moments because of the spin polarization of the 3*d* electrons in the transition metal[14]. However, the origin of ferromagnetism in transition metal doped lead-free ferroelectric materials were still debated. The pure $Na_{0.5}Bi_{0.5}TiO_3$ materials exhibited the weak-ferromagnetism at room temperature which were possible explained by the surface-effect and/or self-defect[15,16]. Zhang et al. predicted that Na and Ti vacancies induced the magnetization rather than Bi or O vacancies[15]. Ju et al. reported that Na vacancies located at/near the surface of nanograins of nanocrystalline $Na_{0.5}Bi_{0.5}TiO_3$ materials possibly displayed the ferromagnetism[16]. Such predictions were well consisted with recent obtained room temperature ferromagnetism in pure $Na_{0.5}Bi_{0.5}TiO_3$ materials[10,11]. However, the magnetization of pure $Na_{0.5}Bi_{0.5}TiO_3$ materials are quite small,

[1]School of Engineering Physics, Ha Noi University of Science and Technology, 1 Dai Co Viet road, Ha Noi, Viet Nam. [2]Department of Physics, University of Ulsan, Ulsan 680-749, Republic of Korea. [3]School of Electronics and Telecommunications, Ha Noi University of Science and Technology, 1 Dai Co Viet road, Ha Noi, Viet Nam. [4]Department of Physics, Incheon National University, Incheon 22012, South Korea. ✉email: dung.dangduc@hust.edu.vn; duc.nguyenvan1@hust.edu.vn; yskim2@ulsan.ac.kr; odkhuu@inu.ac.kr

normally less than 1 memu/g, which hinted to apply in electronics devices. Injection of transition metal into host lead-free ferroelectric $Na_{0.5}Bi_{0.5}TiO_3$ materials possibly enhanced the magnetization up to ~ 9 memu/g[10]. Unlikely the picture of ferromagnetism at room temperature of pure $Na_{0.5}Bi_{0.5}TiO_3$, a various magnetism sources were injected to lead-free ferroelectric materials which resulted in the room temperature ferromagnetism; such as the O-vacancies (in case of Cr-doped $Na_{0.5}Bi_{0.5}TiO_3$), magnetic clusters (in case of Co-doped $Na_{0.5}Bi_{0.5}TiO_3$), or interaction of magnetic cations through oxygen vacancies as intrinsic phenomenon (in case of Fe-, Mn-doped $Na_{0.5}Bi_{0.5}TiO_3$)[8–11]. Therefore, the origin of room temperature ferromagnetism needs to be deep understood to control the magnetization for smart-electronic devices application.

Thank to well solid solution of $Na_{0.5}Bi_{0.5}TiO_3$ material with various type of ABO_3 dopant materials, the physical properties of host $Na_{0.5}Bi_{0.5}TiO_3$ materials were enhanced[17–27]. Rahman et al. reported that both ferroelectric and piezoelectric properties of $Na_{0.5}Bi_{0.5}TiO_3$ increased via solid solution of $BaZrO_3$ where the both remanent polarization and piezoelectric constant increased from 22 μC/cm^2 and 60 pC/N for pure $Na_{0.5}Bi_{0.5}TiO_3$ to 30 μC/cm^2 and 112 pC/N for 4 mol% $BaZrO_3$ solid solution in $Na_{0.5}Bi_{0.5}TiO_3$ materials[17]. Yang et al. reported that the $(Ba_{0.7}Ca_{0.3})TiO_3$ solid solution in host $Na_{0.5}Bi_{0.5}TiO_3$ materials resulted in greatly lowered coercive field without degrading remanent polarization[18]. Bai et al. reported that the $Bi(Me_{0.5}Ti_{0.5})O_3$ (Me = Zn, Ni, Mg, Co)-modified $Na_{0.5}Bi_{0.5}TiO_3$ materials displayed the large strain response (> 0.3%) with a high normalized strain S_{max}/E_{max} (> 550 pm/V)[19]. Zhou et al. reported that $BaNb_2O_6$ diffused into lattice of $Na_{0.5}Bi_{0.5}TiO_3$ to form a solid solution resulted in enhancement of the dielectric properties of host $Na_{0.5}Bi_{0.5}TiO_3$ materials[20]. Kaswan et al. reported on ferromagnetism in $Bi_{0.5}Na_{0.5}TiO_3$-$Bi_{0.8}Ba_{0.2}FeO_3$ composite materials[21]. Pattanayak et al. observed the ferromagnetic properties of a $BaFe_{12}O_{19}$-modified $Bi_{0.5}Na_{0.5}TiO_3$ system[22]. Recently, Singh et al. reported on the ferromagnetic properties of $Bi_{0.5}Na_{0.5}TiO_3$ materials induced by the addition of $LaFeO_3$ as solid solution[23]. In addition, the magnetic properties of $Na_{0.5}Bi_{0.5}TiO_3$ materials were found to be strong enhancement such magnetization via solid solution with various impurities materials such as ilmenite-type materials (e.g. $MnTiO_3$, $NiTiO_3$, $FeTiO_3$, or $CoTiO_3$), or perovskite-type materials (e.g. $MgFeO_{3-\delta}$, $SrFeO_{3-\delta}$, $CaFeO_{3-\delta}$, $SrMnO_{3-\delta}$, $CaMnO_{3-\delta}$, $BaMnO_{3-\delta}$, $MgMnO_{3-\delta}$, $SrCoO_{3-\delta}$, $MgCoO_{3-\delta}$, $BaCoO_{3-\delta}$, or $CaCoO_{3-\delta}$)[24–38]. The double perovskite-type structural materials containing the transition metals (e.g. $Bi(Ti_{0.5}Fe_{0.5})O_{3-\delta}$, $Bi(Ti_{0.5}Mn_{0.5})O_{3-\delta}$, $Bi(Ti_{0.5}Co_{0.5})O_{3-\delta}$, or $Bi(Ti_{0.5}Ni_{0.5})O_{3-\delta}$) were also reported to enhance the magnetic properties of $Na_{0.5}Bi_{0.5}TiO_3$ materials when their materials were solid solution into host materials[39–42]. The magnetization of modified- $Na_{0.5}Bi_{0.5}TiO_3$ samples via impurities of ilmenite-type materials, perovskite-type or double perovskite-type structural materials were found to have large magnetization moment which were compared with single transition metal dopants[8–11,24–42].

Among alkaline-earth iron perovskite $AeFeO_{3-\delta}$ family (Ae = Ba, Ca, Sr, and Mg), $BaFeO_{3-\delta}$ is one of interesting materials because its ferromagnetic domains could be controllable by an applied magnetic field[43]. $BaFeO_{3-\delta}$ materials exhibited complex of phase such as monoclinic, rhombohedral, pseudo-cubic and cubic which depended on the valence state of Fe and transition between them[44]. Mori et al. reported that $BaFeO_{3-\delta}$ compounds existed in many forms such hexagonal phase in a wide range of oxygen content $BaFeO_{2.63-2.92}$ while other phase has exhibited such triclinic I, $BaFeO_{2.50}$; triclinic II, $BaFeO_{2.64-2.67}$; rhombohedral I and II, $BaFeO_{2.62-2.64}$; and tetragonal, $BaFeO_{2.75-2.81}$[45]. The cubic perovskite $BaFeO_3$ with Fe^{4+} state has A-type spiral spin structure as ferromagnetism below 111 K[46]. Clemens et al. reported that $BaFeO_{2.5}$ materials with Fe^{3+} state exhibited the G-type antiferromagnetic structure with Neel temperature of 720 K[47]. Delattre et al. reported that the $BaFeO_{2.8}$ with orthorhombic structural exhibited the strong couple antiferromagnet[48]. Theoretical simulation predicted that the $BaFeO_2$ materials has tetragonal symmetry and the G-type antiferromagnetic spin configuration[49]. The highest ferromagnetic ordering around 235 K in $BaFeO_{3-\delta}$ were obtained for thin film growing on the $SrTiO_3$ substrate[50]. Recently, the new system of $(1-x)Na_{0.5}Bi_{0.5}TiO_3 + xAeFeO_{3-\delta}$ (Ae = Sr, Ca, and Mg) materials as solid solution were successful fabricated by using the sol–gel technique[28–30]. The results provided that the impurities cation (such as Sr, Mg) and Fe random incorporated with (Bi,Na)-site and Ti-site, respectively, were exhibited the strong ferromagnetism at room temperature where the magnetization were found to great enhancement than that of single transition metal dopants which were possible resulted from co-modification at A-site via alkaline-earth and Fe cation at B-site of host $Na_{0.5}Bi_{0.5}TiO_3$[28–30]. In the periodic table of elements, Ba is the largest radius in alkaline earth metals, thus, we expected that the co-modification of Ba cations at A-site and Fe cations at B-site, respectively, of host $Na_{0.5}Bi_{0.5}TiO_3$ materials were resulted exhibition large magnetization during solid solution of $BaFeO_{3-\delta}$ into $Na_{0.5}Bi_{0.5}TiO_3$ materials.

In this work, new system $(1-x)Na_{0.5}Bi_{0.5}TiO_3 + xBaFeO_{3-\delta}$ materials as solid solution were fabricated by sol–gel method. The $BaFeO_{3-\delta}$ materials were well solid solution into the host $Na_{0.5}Bi_{0.5}TiO_3$ materials through diffusion and random incorporation of Ba and Fe cations with host lattice of $Na_{0.5}Bi_{0.5}TiO_3$ materials. The structural distortion and reduced optical band gap of host $Na_{0.5}Bi_{0.5}TiO_3$ materials were obtained. The complex magnetic properties of $BaFeO_{3-\delta}$-modified $Na_{0.5}Bi_{0.5}TiO_3$ materials was obtained as function of $BaFeO_{3-\delta}$ amounts addition.

Results and discussion

Figure 1a,b shows the EDS spectral of pure $Na_{0.5}Bi_{0.5}TiO_3$ samples and $BaFeO_{3-\delta}$-modified $Na_{0.5}Bi_{0.5}TiO_3$ sample with 5 mol.% $BaFeO_{3-\delta}$, respectively. The inset of each figure showed the selected area for EDS elements characterization. All expectational elements such Bi, Na, Ti and O were obtained in EDS spectral of pure $Na_{0.5}Bi_{0.5}TiO_3$ samples, as shown in Fig. 1a. The addition of the Ba and Fe peaks were showed in the EDS spectral of $BaFeO_{3-\delta}$-modified $Bi_{0.5}Na_{0.5}TiO_3$ samples, as expected, which were presented at the Fig. 1b. The results provided that the $BaFeO_{3-\delta}$ impurities existed in our samples.

The chemical maps of $Bi_{0.5}Na_{0.5}TiO_3$ materials modified with 9 mol.% $BaFeO_{3-\delta}$ were analyzed. The distribution of impurity elements in the $Na_{0.5}Bi_{0.5}TiO_3$ materials modified with 9 mol.% $BaFeO_{3-\delta}$ is shown in Fig. 2. The surface morphology of the area selected for chemical mapping is shown in Fig. 2a, whereas Fig. 2b presents the total contribution of all of the chemical elements in the sample. The partial chemical maps of Bi, Na, Ti, O,

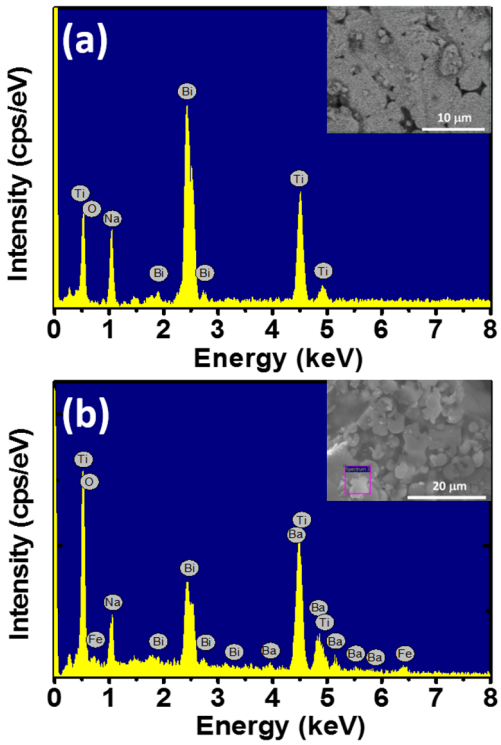

Figure 1. The EDS spectral of **(a)** pure $Na_{0.5}Bi_{0.5}TiO_3$ materials, and **(b)** $BaFeO_{3-\delta}$-modified $Na_{0.5}Bi_{0.5}TiO_3$ materials with 5 mol% $BaFeO_{3-\delta}$ as solid solution. The inset of each figure shown the selected area for composition characterization.

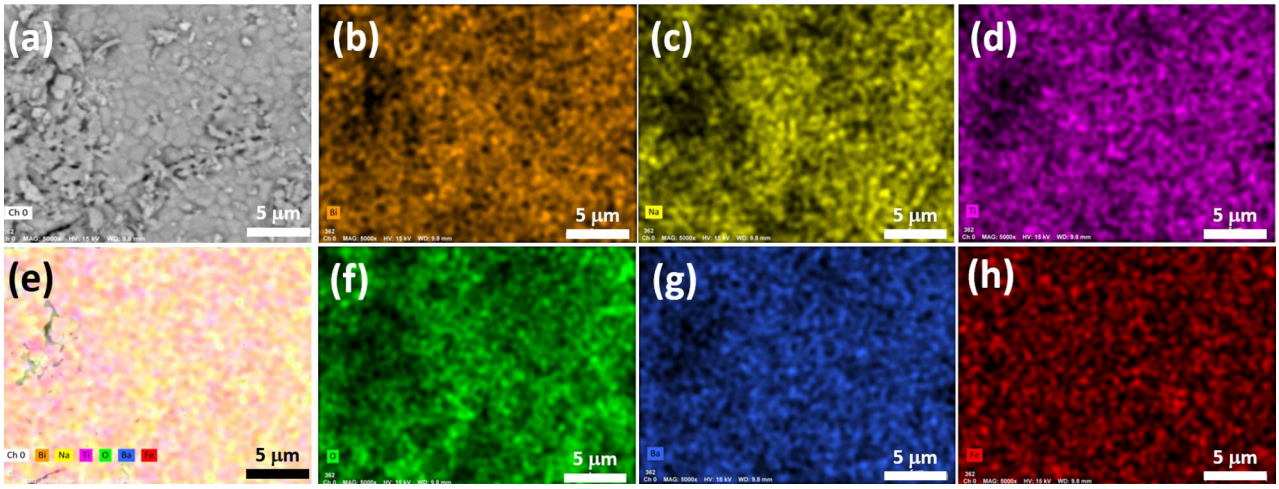

Figure 2. **(a)** Selected area for the chemical mapping of 9 mol.% $BaFeO_{3-\delta}$-modified $Na_{0.5}Bi_{0.5}TiO_3$ materials; **(b)** total chemical element distribution in samples; and (c)–(h) partial chemical element maps of Bi, Na, Ti, O, Ba, and Fe.

Ba, and Fe elements are shown in Fig. 2c–h, respectively. The results clearly demonstrated that the constituent chemical elements were homogenously dispersed in the sample.

Figure 3 (a) shows the X-ray diffraction patterns of pure $Na_{0.5}Bi_{0.5}TiO_3$ and $BaFeO_{3-\delta}$-modified $Na_{0.5}Bi_{0.5}TiO_3$ with various $BaFeO_{3-\delta}$ concentrations. On the basis of diffraction peak position and relative to intensity, all samples were indexed to a perovskite structure with the rhombohedral symmetry of the $Na_{0.5}Bi_{0.5}TiO_3$ compound (JCPDS card no. 00–036-0340, space group R3c). In addition, the impurities phase or phase segregation was not founded in the X-ray diffraction patterns. All X-ray diffraction pattern of $BaFeO_{3-\delta}$-modified $Na_{0.5}Bi_{0.5}TiO_3$ samples were indexed to follow the structural of $Na_{0.5}Bi_{0.5}TiO_3$ compound. The results indicated that $BaFeO_{3-\delta}$ materials exhibited a well solid solution in $Na_{0.5}Bi_{0.5}TiO_3$ materials. In other word, the Ba and Fe cations were diffused to randomly incorporate with host lattice of $Na_{0.5}Bi_{0.5}TiO_3$ compound as solid solution. In order to

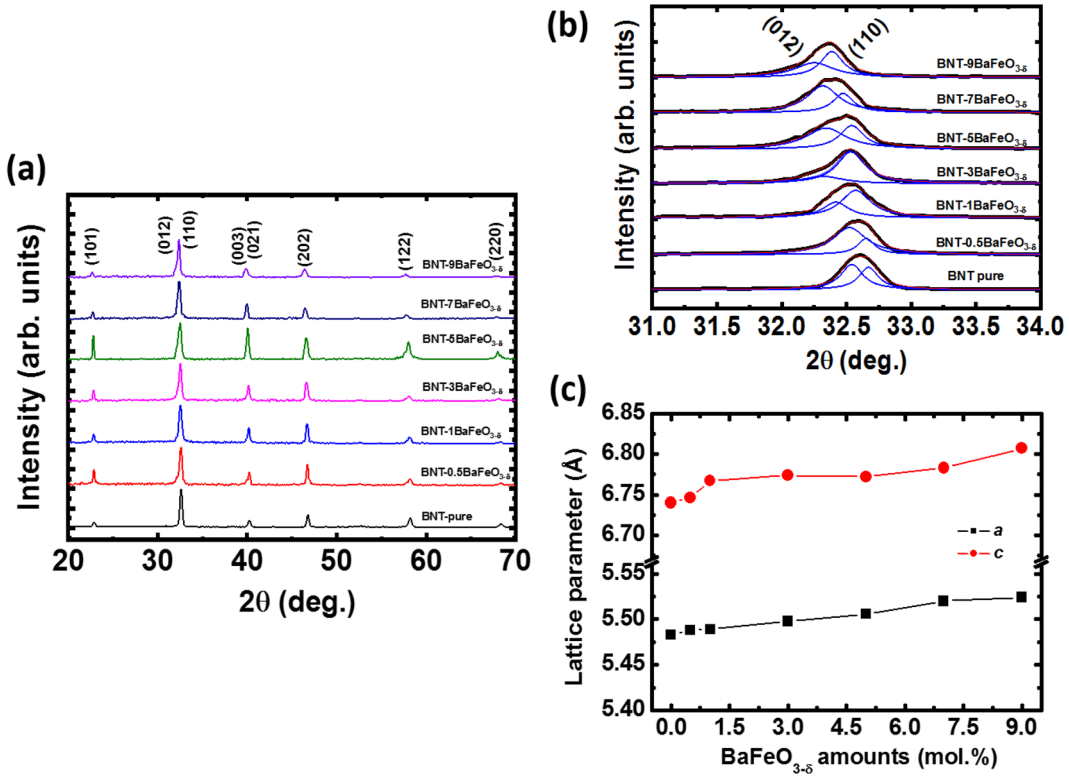

Figure 3. **(a)** X-ray diffraction pattern of $BaFeO_{3-\delta}$ solid solution into $Na_{0.5}Bi_{0.5}TiO_3$ with various concentrations within the 2θ range of 20° to 70°; **(b)** magnified X-ray diffraction within 2θ range of 31°–34° for comparing setline (012)/(110) peaks; and **(c)** dependence of the lattice parameters of pure $Bi_{0.5}Na_{0.5}TiO_3$ and $BaFeO_{3-\delta}$-modified $Bi_{0.5}Na_{0.5}TiO_3$ samples on the amounts of $BaFeO_{3-\delta}$ solid solution.

character the influence of Ba and Fe into host crystalline of $Na_{0.5}Bi_{0.5}TiO_3$ compound, the diffraction angle of pure $Na_{0.5}Bi_{0.5}TiO_3$ and $BaFeO_{3-\delta}$-modified $Bi_{0.5}Na_{0.5}TiO_3$ samples was magnified within 31.0° to 34.0° for setline (012)/(110) peaks, as shown in Fig. 3b. The setline peaks were overloaded together which were distinguished via Lorentz fitting, as shown in dot line of Fig. 3b. The results clearly indicated that the diffraction peaks of $Na_{0.5}Bi_{0.5}TiO_3$ materials trended to shift to lower diffraction angle as increasing the $BaFeO_{3-\delta}$ amounts, which provided the evident for expansion of lattice parameter. Furthermore, the lattice parameters *a* and *c* of the pure $Bi_{0.5}Na_{0.5}TiO_3$ and the $BaFeO_{3-\delta}$-modified $Bi_{0.5}Na_{0.5}TiO_3$ as a function of $BaFeO_{3-\delta}$ addition amounts are shown in Fig. 3c. The results show that the distorted lattice parameters of the $Bi_{0.5}Na_{0.5}TiO_3$ compound are not a linear function of the concentrations of the $BaFeO_{3-\delta}$ solid solution, which showed complex lattice parameter distortion. This result could be attributed to the different radii of Ba and Fe cations in the additives and that of Bi, Na, and Ti incorporated randomly in the lattice of the host $Na_{0.5}Bi_{0.5}TiO_3$ materials. Based on the Shamon' reported, the radius of Ba^{2+} and $Fe^{2+/3+}$ cations were 1.61 Å and 0.645 Å/0.780 Å, respectively, while the radius of Bi^{3+}, Na^+ and Ti^{4+} cations were 1.17 Å, 1.39 Å and 0.605 Å, respectively[51]. Therefore, the Fe cations diffused to substitute for Ti-sites in perovskite structural of $Na_{0.5}Bi_{0.5}TiO_3$ crystal, resulted in expansion of the lattice. The fact that the radius of Ba^{2+} cations are larger than that of both Bi^{3+} and Na^+ cations were also reflected by expanding the lattice parameter of host $Na_{0.5}Bi_{0.5}TiO_3$ compound. However, we noted that the oxygen vacancies were generated due to unbalance of valence states of $Fe^{2+/3+}$ and Ti^{4+} at *B*-site and Ba^{2+} for Bi^{3+} at *A*-site. In addition, the Na vacancies were created when Ba^{2+} substitute Na^+. The oxygen vacancies (¤) has radius of 1.31 Å which were smaller than that of oxygen anion (O^{2-}) of 1.4 Å[52]. Therefore, the existence of oxygen vacancies in the structure led to reduction of the lattice parameter. The structural distortion of $Na_{0.5}Bi_{0.5}TiO_3$ materials was due to co-modification at *A*- and *B*-site via alkali earth and transition metal, respectively, which was consistent with recently reported[28–30]. In other word, the X-ray diffraction characterization of $BaFeO_{3-\delta}$-modified $Na_{0.5}Bi_{0.5}TiO_3$ samples provided that the $BaFeO_{3-\delta}$ materials were well solid solution into host $Na_{0.5}Bi_{0.5}TiO_3$ materials.

Figure 4a show the Raman scattering of pure $Na_{0.5}Bi_{0.5}TiO_3$ materials and $BaFeO_{3-\delta}$-modified $Na_{0.5}Bi_{0.5}TiO_3$ materials with various of $BaFeO_{3--\delta}$ concentration as solid solutions at room temperature. The results provide that the shape of Raman scattering spectra seem to be unchanged in comparison between that of pure $Na_{0.5}Bi_{0.5}TiO_3$ materials and that of $BaFeO_{3-\delta}$-modified $Na_{0.5}Bi_{0.5}TiO_3$ s materials. In the wave number ranging from 300 cm^{-1} to 1000 cm^{-1}, the Raman spectra were possible divided into three main regions and they overlapped each other. The three main band regions were in the range of 300–450 cm^{-1}, 450–700 cm^{-1} and 700–1000 cm^{-1}, respectively. The combination of experimental investigation and first principles density functional theoretical calculation for Raman vibration modes of $Na_{0.5}Bi_{0.5}TiO_3$ materials exhibited that the lowest frequency modes in range of

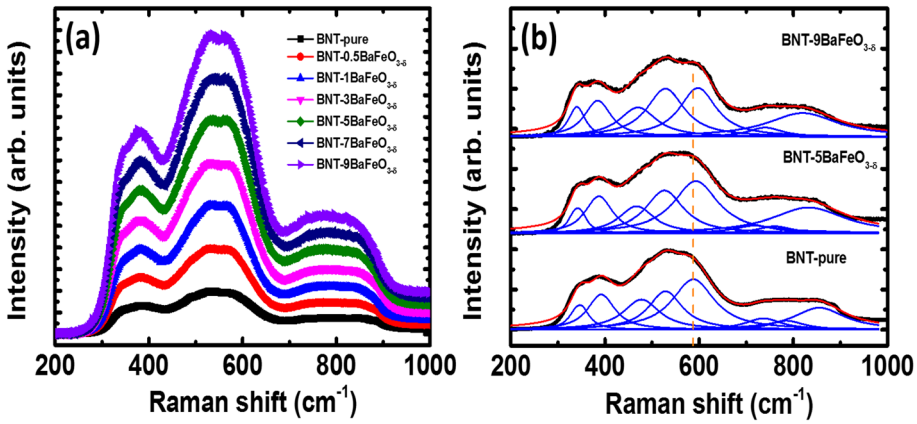

Figure 4. **(a)** Raman scattering spectra of $BaFeO_{3-\delta}$ solid solution into $Na_{0.5}Bi_{0.5}TiO_3$ with various concentrations from 200 cm^{-1} to 1000 cm^{-1}; and **(b)** deconvolution Raman peaks of pure $Na_{0.5}Bi_{0.5}TiO_3$ and 5 and 9 mol% $BaFeO_{3-\delta}$ solid solution into $Na_{0.5}Bi_{0.5}TiO_3$.

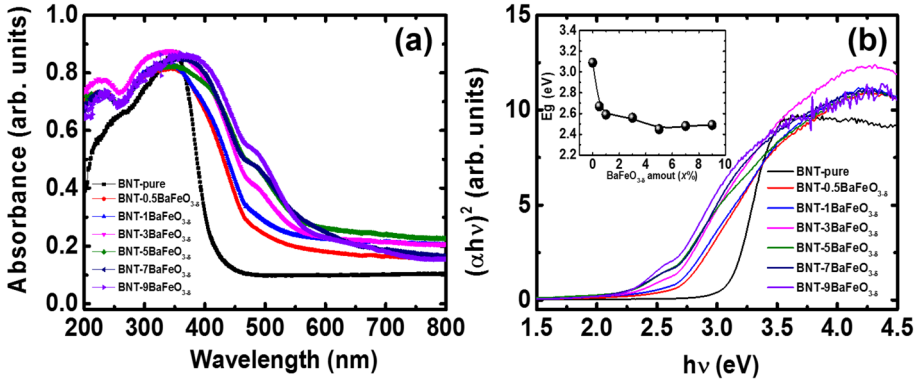

Figure 5. **(a)** UV–Vis absorption spectra of $BaFeO_{3-\delta}$-modified $Na_{0.5}Bi_{0.5}TiO_3$ samples as a function of $BaFeO_{3-\delta}$ concentration; and **(b)** the $(\alpha h\nu)^2$ proposal with photon energy ($h\nu$) of $Na_{0.5}Bi_{0.5}TiO_3$ samples as a function of the amount of $BaFeO_{3-\delta}$ added. The inset of **(b)** shows the optical band gap E_g value of $Na_{0.5}Bi_{0.5}TiO_3$ samples as a function of the amount of $BaFeO_{3-\delta}$ added.

246–401 cm^{-1} are dominated by TiO_6 vibrations, and the higher frequency modes in the range 413–826 cm^{-1} are primarily associated with the oxygen atoms vibrations[53]. The random occupation at *A*-sites of Bi and Na resulted in overlap of Raman scattering peaks in range of 109–134 cm^{-1} and 155–187 cm^{-1}, which were originated from Bi-O and Na–O vibration modes, respectively[53]. In addition, Chen et al. reported that the vibration of Ti–O bonds is related to the wave number in range of 200–400 cm^{-1} while the vibration of TiO_6 octahedra is assigned to the wave number regions from 450 cm^{-1} to 700 cm^{-1}[54]. The overlapping of Raman scattering modes was hard to characterize the influence of Ba and Fe into vibration modes of host lattice $Na_{0.5}Bi_{0.5}TiO_3$ materials. Therefore, we tried to distinguish the Raman scattering modes via the fitting with Lorentz functions (with correction of fitting over 0.99). The deconvolution Raman scattering modes (blue line) of pure $Na_{0.5}Bi_{0.5}TiO_3$ samples and $BaFeO_{3-\delta}$-modified $Na_{0.5}Bi_{0.5}TiO_3$ samples with example for 5 and 9 mol% $BaFeO_{3-\delta}$, as shown in Fig. 4b. The eight Raman scattering vibrational modes were obtained for both pure $Na_{0.5}Bi_{0.5}TiO_3$ and $BaFeO_{3-\delta}$-modified $Na_{0.5}Bi_{0.5}TiO_3$ samples. The results were well consistent with recently observation in vibration of Raman scattering modes of perovskite-type structural $AeFeO_{3-\delta}$ family-modified $Na_{0.5}Bi_{0.5}TiO_3$ materials[28–30]. The vibration modes at around 595 cm^{-1} (red dot line marked in the Fig. 4b) trended to shift to high frequency, which were suggested to be related to distorted structure of $(Ti,Fe)O_6$ framework and/or effective mass effect because of difference between the radius and mass of impurities Fe and host Ti at *B*-site[28–30]. In other word, the shifted Raman scattering modes confirmed the substitution of Ba and Fe into the host lattice of $Na_{0.5}Bi_{0.5}TiO_3$ materials.

Figure 5a shows the optical absorption spectra of pure $Na_{0.5}Bi_{0.5}TiO_3$ and $BaFeO_{3-\delta}$-modified $Na_{0.5}Bi_{0.5}TiO_3$ with various $BaFeO_{3-\delta}$ concentrations. Pure $Na_{0.5}Bi_{0.5}TiO_3$ samples exhibited a single absorbance edge, consistent with the reported optical properties of $Na_{0.5}Bi_{0.5}TiO_3$ materials[9–11,55]. However, pure $Na_{0.5}Bi_{0.5}TiO_3$ materials exhibited the unsharp transition which were tailored with slightly tail. The small tail at long wavelength in absorbance spectroscopy of pure $Na_{0.5}Bi_{0.5}TiO_3$ materials were suggested to be related with self-defect and/or surface effect cause of unsaturation bonding pair of atoms at the surface[55,56]. The addition $BaFeO_{3-\delta}$ to $Na_{0.5}Bi_{0.5}TiO_3$ material as solid solution led to a red shift of the absorbance edge. The appearance of peaks around 485 nm in

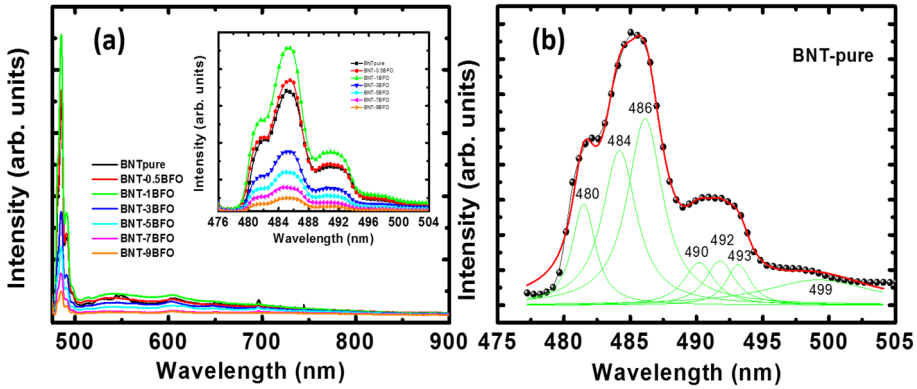

Figure 6. **(a)** PL spectral of pure $Bi_{0.5}Na_{0.5}TiO_3$ materials and $BaFeO_{3-\delta}$-modified $Na_{0.5}Bi_{0.5}TiO_3$ samples as a function of $BaFeO_{3-\delta}$ concentration, and **(b)** deconvolution of PL spectral of pure $Bi_{0.5}Na_{0.5}TiO_3$ materials. The inset of **(a)** shown the magnification of PL spectral of pure and $BaFeO_{3-\delta}$-modified $Na_{0.5}Bi_{0.5}TiO_3$ samples as a function of $BaFeO_{3-\delta}$ concentration.

the absorbance spectra of $BaFeO_{3-\delta}$-modified $Na_{0.5}Bi_{0.5}TiO_3$ materials indicated the new local states of Fe cations in the middle electronic band structure of $Na_{0.5}Bi_{0.5}TiO_3$ materials[28–30,57]. Optical band gap (E_g) values of pure $Na_{0.5}Bi_{0.5}TiO_3$ and $BaFeO_{3-\delta}$-modified $Na_{0.5}Bi_{0.5}TiO_3$ materials were calculated using the plot of $(\alpha h\nu)^2$ versus photon energy $h\nu$, as shown in Fig. 5b, where α, h and ν are the absorbance coefficient, the Planck constant and the frequency, respectively. The band gap energy of pure $Na_{0.5}Bi_{0.5}TiO_3$ materials were estimated to be approximately 3.09 eV, whereas that of $BaFeO_{3-\delta}$-modified $Na_{0.5}Bi_{0.5}TiO_3$ materials exhibited value of 2.48 eV for 9 mol. % $BaFeO_{3-\delta}$ solid solution in host $Na_{0.5}Bi_{0.5}TiO_3$ materials. The detail dependence of E_g values of $BaFeO_{3-\delta}$-modified $Na_{0.5}Bi_{0.5}TiO_3$ compound as function of $BaFeO_{3-\delta}$ concentration is shown in the inset of Fig. 5b. The optical band gap of $Na_{0.5}Bi_{0.5}TiO_3$ material in which the Ti-sites substituted with the transition metal, as *B*-site modified, decreased in lead-free ferroelectric Bi-based materials; this phenomenon could be due to the presence of new local states in the electronic structure of both the highest occupied molecular orbital and the lowest unoccupied molecular orbital in the total band structure[9–11,14,57]. In addition, the reduced optical band gap in *A*-site modified $Na_{0.5}Bi_{0.5}TiO_3$-based material was possibly a result of changes in the bonding type between hybridizations *A*-O[58]. Oxygen vacancies created because of unbalanced charges between impurities and hosts (e.g. $Fe^{2+/3+}$ substitute for Ti^{4+}, and Ba^{2+} replacement for Bi^{3+}) also led to the reduction in the optical band gap because the oxygen vacancy states normally located below and near the conduction band[9–11,59,60]. Thus, we suggest that the random substitution of Ba and Fe ions into the host $Na_{0.5}Bi_{0.5}TiO_3$ could alter the electronic band structure, resulting in reduction of the optical band gap.

Figure 6a shows the room-temperature PL emission spectra of pure $Na_{0.5}Bi_{0.5}TiO_3$ and $BaFeO_{3-\delta}$-modified $Na_{0.5}Bi_{0.5}TiO_3$ samples with various $BaFeO_{3-\delta}$ amount. The PL spectral of all samples exhibited a broad band emission while strong emission showed in range from 479 to 505 nm. The addition of $BaFeO_{3-\delta}$ into host $Na_{0.5}Bi_{0.5}TiO_3$ materials as solid solution suppressed the emission peak, as shown in inset of Fig. 6a. However, we noted that a slight addition of $BaFeO_{3-\delta}$ concentration enhanced the emission intensity. In addition, the PL spectral of pure $Na_{0.5}Bi_{0.5}TiO_3$ and $BaFeO_{3-\delta}$-modified $Na_{0.5}Bi_{0.5}TiO_3$ samples was overlapped together, suggesting to multi-emission peaks with closed together. Thus, we tried to distinguish the multi-emission peaks via Lorentz fitting. The deconvoluted emission peaks of pure $Na_{0.5}Bi_{0.5}TiO_3$ samples were shown in Fig. 6b. The broad band visible luminescence was also recently reported for ferroelectric titanates-based materials at room temperature such as $BaTiO_3$, $SrTiO_3$, $PbTiO_3$ etc.[61]. The observations in broad band emission were also archived in $Bi_{0.5}K_{0.5}TiO_3$ materials, which were related to the surface effect and/or self-defect effect[56]. Normally, the coordination status of the atoms at the surface of materials is unsaturated, resulting in unpaired states, that make them different from that in the bulk[62]. The unsaturated atoms that existed at the surface region of $Na_{0.5}Bi_{0.5}TiO_3$ materials formed local levels in the forbidden gaps, this displayed the effect of the self-trapped excitons[63]. Therefore, the incident photon was absorbed by the $Na_{0.5}Bi_{0.5}TiO_3$ powder as it is illuminated with the excited source. The absorption photons could create some localized levels and form small polarons. The interaction between the holes in the valence band and polarons formed by the intermediate self-trapped excitons caused blue shift of the luminescence[63]. In addition, the structural distortion because of coupling of TiO_6-TiO_6 adjacent octahedra generate the localized electronic levels above the valence band. The recombination from these levels may result in the photoluminescence of $Bi_{0.5}K_{0.5}TiO_3$ materials[62]. The photoluminescence of ferroelectric materials is not generally governed by band-to-band transition, owning to the difficulty in recombination of electron–hole pairs and the separation of the natural polarization domain in the materials. In this kind of materials, the surface states were in charge of the luminescence, in which many unsaturated atoms that presented on the surface of the ferroelectric materials creates the localized levels in the forbidden gaps. Interestingly, the intensity of PL emission of $Na_{0.5}Bi_{0.5}TiO_3$ materials was suppressed by the addition of $BaFeO_{3-\delta}$, as shown in the inset of Fig. 6b. The PL emission spectra of $BaFeO_{3-\delta}$-modified $Na_{0.5}Bi_{0.5}TiO_3$ materials did not change, indicating the lack of Ba and Fe substitution at the *A*- and *B*-sites, respectively, in the new electron–hole transitions. Thus, the substitution of Fe cation with Ti at the octahedral sites created oxygen vacancies; such vacancies acted as the chapping electron

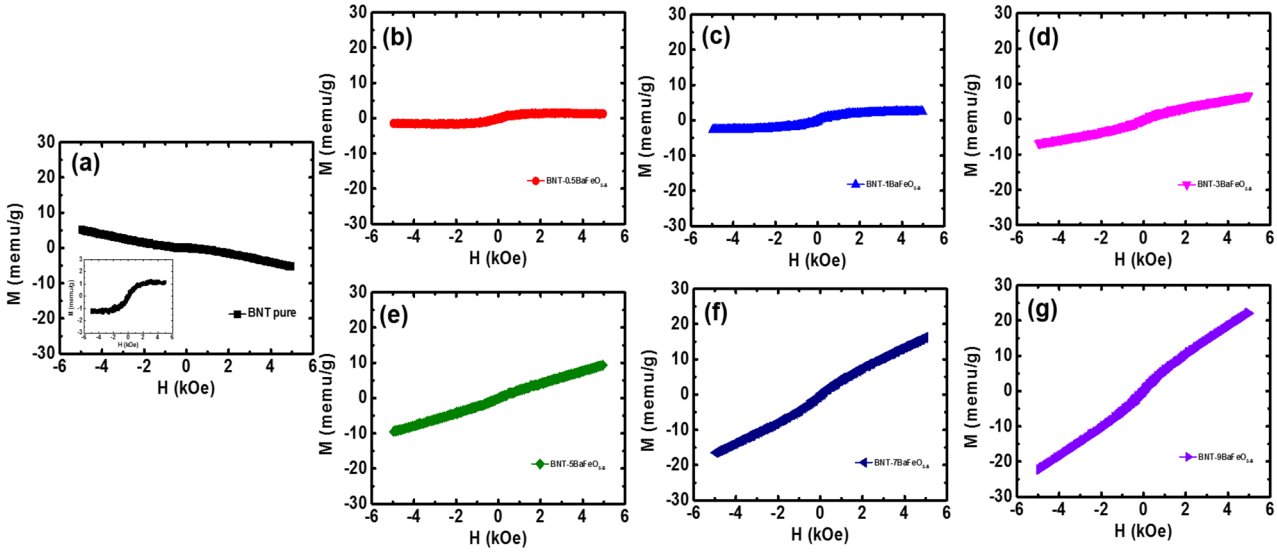

Figure 7. *M–H* curves at room temperature of **(a)** undoped $Na_{0.5}Bi_{0.5}TiO_3$, and $BaFeO_{3-\delta}$-modified $Na_{0.5}Bi_{0.5}TiO_3$ samples with **(b)** 0.5 mol%, **(c)** 1 mol%, **(d)** 3 mol%, **(e)** 5 mol%, **(f)** 7 mol% and **(g)** 9 mol% $BaFeO_{3-\delta}$ as solid solution. Inset of **(a)** shown the M-H curve of pure $Bi_{0.5}Na_{0.5}TiO_3$ material after substrate diamagnetic components.

generated from absorbance photon energy, thereby prevented the recombination of the electron–hole pairs to generate photons.

Furthermore, the role of $BaFeO_{3-\delta}$ solid solution in $Na_{0.5}Bi_{0.5}TiO_3$ materials in imparting magnetism was dependent on the applied magnetic field at room temperature, as shown in Fig. 7a–g for pure $Na_{0.5}Bi_{0.5}TiO_3$ and $BaFeO_{3-\delta}$-modified $Na_{0.5}Bi_{0.5}TiO_3$ materials with $BaFeO_{3-\delta}$ concentration of 0.5, 1, 3, 5, 7 and 9 mol%, respectively. The pure $Na_{0.5}Bi_{0.5}TiO_3$ exhibited the anti-*S*-shape in *M-H* curves, indicating the combination of diamagnetism and weak ferromagnetism, as shown in Fig. 7a. The diamagnetism in pure $Na_{0.5}Bi_{0.5}TiO_3$ samples originated from the electronic configuration of Ti^{4+} as $3d^o$, whereas the weak ferromagnetism originated from self-def ects[9–11,14,16,30,64,65]. The typical hysteresis loop of ferromagnetism was obtained for pure $Na_{0.5}Bi_{0.5}TiO_3$ materials after subtract the diamagnetic components, as shown in inset of Fig. 7a. The saturation magnetization was estimated around 1.5 memu/g which were well consisted with recently reported by Ju et al.[16]. In addition, the remanent magnetization (M_r) and coercive field (H_C) of pure $Na_{0.5}Bi_{0.5}TiO_3$ materials were approximately 0.11 memu/g and 73 Oe, respectively, which were solid evidence for presentation of ferromagnetic state at room temperature. The estimation for their values were also performed with recently reported by Thanh et al. and Ju et al. which those were possibly originated from self-defect such as Na-, Ti- or O-vacancies[10,16]. The *M-H* curves trend to switch from anti-*S*-shape to *S*-shape in the $BaFeO_{3-\delta}$-modified $Na_{0.5}Bi_{0.5}TiO_3$ samples as the $BaFeO_{3-\delta}$ concentration in the solid solution increase, providing evidence regarding the strength enhancement of ferromagnetic ordering in the samples. As shown in Fig. 7c, the typical ferromagnetic hysteresis loops were obtained where the magnetization trended to saturate as the external applied magnetic field increase, and the strength of ferromagnetic increase. However, further increasing amounts of $BaFeO_{3-\delta}$ into host $Na_{0.5}Bi_{0.5}TiO_3$, the *M-H* curves exhibited the unsaturation with low applied external magnetic field, as shown in Fig. 7d–g. The dependence of shape in magnetic hysteresis loop of $BaFeO_{3-\delta}$-modified $Na_{0.5}Bi_{0.5}TiO_3$ materials represented that the magnetic properties of $BaFeO_{3-\delta}$-modified $Na_{0.5}Bi_{0.5}TiO_3$ materials were very complex, on the one hand the magnetic properties of $Na_{0.5}Bi_{0.5}TiO_3$ materials were strong dependent of the concentration of $BaFeO_{3-\delta}$ as solid solution. The M_r and H_C values of $BaFeO_{3-\delta}$-modified $Bi_{0.5}Na_{0.5}TiO_3$ materials were approximately 51–106 Oe and 0.12–0.48 memu/g, respectively. These results were consistent with the recently observed M_r and H_C of transition-metal-doped lead-free and lead-based ferroelectric materials[8–11,60,64–68]. The nonzero M_r and H_C values of $BaFeO_{3-\delta}$-modified $Bi_{0.5}Na_{0.5}TiO_3$ materials provided solid evidence for the presence of the ferromagnetic state at room temperature. In additon, the maximum magnetization was estimated around 23 memu/g for 9 mol% $BaFeO_{3-\delta}$ solid solution in host $Na_{0.5}Bi_{0.5}TiO_3$ materials. That value was larger than that of self-defect induced magnetism of pure $Na_{0.5}Bi_{0.5}TiO_3$ materials or single transition metals doped $Na_{0.5}Bi_{0.5}TiO_3$ materials, in which around ~ 1.5 memu/g for Cr-doped $Na_{0.5}Bi_{0.5}TiO_3$, ~ 3 memu/g for Co-doped $Na_{0.5}Bi_{0.5}TiO_3$, ~ 9 memu/g for Mn-doped $Na_{0.5}Bi_{0.5}TiO_3$, ~ 15 memu/g for Fe-doped $Na_{0.5}Bi_{0.5}TiO_3$ materials, and ~ 4 memu/g for Ni-doped $Na_{0.5}Bi_{0.5}TiO_3$ materials[8–11,60,68]. Herein, we need to remark that the origin of ferromagnetism ordering of transition metal impurities containing $Na_{0.5}Bi_{0.5}TiO_3$ materials at room temperature were still debated. The weak-ferromagnetism in pure $Na_{0.5}Bi_{0.5}TiO_3$ materials were possibly originated from self-defect and/or surface defect (such as Ti and Na-vacancies) while the magnetization of $Na_{0.5}Bi_{0.5}TiO_3$ materials were slightly enhanced via oxygen vacancies[11,14,16,30]. The Mn-, Ni- and Fe-doped $Na_{0.5}Bi_{0.5}TiO_3$ materials exhibited the room temperature ferromagnetism which were related to intrinsic phenomenon where the transition cations such of Mn, Ni and Fe interacted with the oxygen vacancies, like *F*-center interaction mechanism, e.g. $Mn^{2+/3+}$–¤–$Mn^{2+/3+}$ or $Fe^{2+/3+}$–¤–$Fe^{2+/3+}$ pairs etc., which were favored for ferromagnetic ordering[8–11,60,64]. Unlikely Mn-, Ni- and

Fe- cations impurities in $Na_{0.5}Bi_{0.5}TiO_3$ materials, the Co impurities trended to form Co-clusters embedding in host $Na_{0.5}Bi_{0.5}TiO_3$ materials which displayed the room temperature ferromagnetism[8]. Recently, our experimental observation along with first principle calculation predicted that the interaction of Co cations into host $Na_{0.5}Bi_{0.5}TiO_3$ materials possibly displayed the weak ferromagnetism at room temperature[64]. In addition, Hung et al. reported that $MgFeO_{3-\delta}$ solid solution in $Na_{0.5}Bi_{0.5}TiO_3$ materials exhibited strong magnetization, which were estimated to be around 39.6 memu/g, where the Mg cations played an importance role for mediating ferromagnetism[28]. The $SrFeO_{3-\delta}$- and$CaFeO_{3-\delta}$-modified $Na_{0.5}Bi_{0.5}TiO_3$ materials also showed strong enhancement of the magnetization at room temperature[29,30]. Note that the Mg cations possibly substituted for both *A*-site (Bi^{3+}, Na^{+}) and *B*-site in $Na_{0.5}Bi_{0.5}TiO_3$ crystal structure while Sr and Ca cations only replaced with *A*-site in host $Na_{0.5}Bi_{0.5}TiO_3$ crystal structure[28–30]. Thus, we suggested that the possible room temperature ferromagnetism in $BaFeO_{3-\delta}$-modified $Na_{0.5}Bi_{0.5}TiO_3$ materials were strongly related to the interaction of Fe cations through oxygen vacancies, like *F*-central interaction, which were recently suggested for Mn-, Ni-, Co- and Fe-doped $Na_{0.5}Bi_{0.5}TiO_3$ materials[9,10,60,64,69]. A recent X-ray photoelectron spectroscopy (XPS) analysis of $CaFeO_{3-\delta}$-modified $Na_{0.5}Bi_{0.5}TiO_3$ materials showed that Fe cations are stable in the Fe^{2+} and Fe^{3+} valence state together with O vacancies[30]. Therefore, we suggest that the interaction pair $Fe^{2+/3+}$–¤–$Fe^{2+/3+}$ favors ferromagnetic ordering[69]. The unsaturation in the *M*–*H* curves of magnetic hysteresis loops of $Na_{0.5}Bi_{0.5}TiO_3$ materials (under 6 kOe of applied magnetic field) as the amount of the $BaFeO_{3-\delta}$ solid solution increase suggested magnetic polaron interaction, wherein the interaction between $Fe^{2+/3+}$–¤–$Fe^{2+/3+}$ versus $Fe^{2+/3+}$–¤–$Fe^{2+/3+}$ resulted in antiferromagnetic-like ordering[9,69–73]. In addition, isolated Fe cations displayed paramagnetic properties[9,69–73]. Thus, the combination of the complex signal of ferromagnetic interaction and antiferromagnetic-like and paramagnetic properties was observed when the $BaFeO_{3-\delta}$ solid solution was present at high concentrations in host $Na_{0.5}Bi_{0.5}TiO_3$ materials. However, unlike single Fe-doped $Na_{0.5}Bi_{0.5}TiO_3$ materials, the modification at *A*-site (Bi^{3+}, Na^{+}) via Ba^{2+} cations in host $Na_{0.5}Bi_{0.5}TiO_3$ materials also possibly contributed a source to the ferromagnetism ordering, in which the substitution of Ba^{2+} cations for Bi^{3+} cations in crystal structure created the O-vacancies while Ba^{2+} cations incorporated for Na^{+} cations generated the Na-vacancies. Both O- and Na- vacancies are origin of the ferromagnetism, but they work in different ways[16,30]. Nevertheless, both the experimental observation and theoretical prediction have agreed that Na-vacancies induce the nonzero magnetic moment[16,30]. Therefore, the strength of magnetic moments can be increased by increasing the number of Na-vacancies. However, unlikely Na-vacancies, the O-vacancies were predicted to be agent of the nonmagnetic moment[30]. The O-vacancies were important in promoting the reduction in valence state from Ti^{4+} to Ti^{3+} (even Ti^{2+}) because of oxygen vacancies bounding surround[30,31,74–76]. The theorey predicted that Ti^{4+} has no magnetic moment whereas the Ti^{3+} or Ti^{2+} have nonzero magnetic moment[30]. Thus, the enhancement in O-vacancies were indirectly induced by the magnetic moment along with the contribution of magnetization of $Ti^{3+/2+}$ defects, resulting in increased magnetic moment that were over the self-defects compared with pure $Na_{0.5}Bi_{0.5}TiO_3$ samples. Recently, XPS results have shown that the Ti^{4+} cations in $Na_{0.5}Bi_{0.5}TiO_3$ materials were possible reduced to Ti^{3+} via modification of $CaFeO_{3-\delta}$- and $SrMnO_{3-\delta}$-modified as solid solution[30,31]. Therefore, we suggested that the increasing the O-vacancies was promoted by the magnetization of self-defect of Ti^{3+} cations. Recently, the interaction between $Co^{3+/2+}$ cations and reduction of valence state of $Ti^{4+-\delta}$ pair through O-vacancies were suggested to favor the ferromagnetic ordering[35]. Therefore, we suggested that the appearance of interaction $Fe^{2+/3+}$–¤–$Ti^{4+-\delta}$ pair may arouse increasing of the strength of ferromagnetic ordering. We recently reported that the magnetic properties of various magnetic compound, such as Mn_2O_3, Mn_5Ge_3 etc., could be tunable by a strain[77,78]. Therefore, due to the difference radius with ions of host lattice, the Ba cations possibly caused a chemical pressure, possibly resulting in the change of interaction between them through oxygen vacancies; finally, resulted in modification of magnetic ordering strength. Recent experimental and theoretical studies have suggested that transition metals may fill *A*- and *B*-sites in the perovskite structure of lead-free ferroelectrics, thus resulting in complex magnetic properties[27,79–83]. Liu et al. reported that $K_{0.45}Na_{0.49}Li_{0.06}NbO_3$ materials modified with Cu at the *A*-site show paramagnetic properties[80]. However, Yang et al. reported that Cu modification at the *B*-site of $EuMnO_3$ materials changes magnetic properties from paramagnetic to antiferromagnetic ordering[81]. Deng et al. found that the paramagnetic properties of $EuMnO_{3-\delta}$ materials were changed to antiferromagnetic via modification at the Eu site by Mn cations[82]. Magnetic phase transition from paramagnetic to antiferromagnetic properties has also been reported for $DyMnO_3$ materials modified with the Mn cation at the Dy-site[83]. Theoretical and experimental studies have suggested that $CoTiO_3$-modified $Na_{0.5}Bi_{0.5}TiO_3$ materials have complex magnetic properties that are strongly dependent on the location of Co impurities at the *A*-site or *B*-sitein the host structure[27,79]. Notably, the radii of $Fe^{2+/3+}$ cations with VIII coordination are 0.92 Å and 0.78 Å, respectively, which are comparable with the radii of Bi^{3+} (1.17 Å) and Na^{+} (1.39 Å) cations[84]. Therefore, we suggested that Fe cations were random incorporated at both the *A*-site and *B*-site likely contributing to the complex magnetic properties of the host $Bi_{0.5}Na_{0.5}TiO_3$ materials. The role of Fe cation substitution at the *A*- and *B*-sites in the magnetic properties of $Na_{0.5}Bi_{0.5}TiO_3$ materials was further investigated by using density-functional theory (DFT) calculation.

To elucidate the origin of the observed ferromagnetism in $BaFeO_{3-\delta}$-doped $Na_{0.5}Bi_{0.5}TiO_3$, the density-functional theory (DFT) calculations were performed using the Vienna ab initio Simulation Package (VASP)[85,86]. The generalized gradient approximation (GGA) formulated by Perdew, Burke, and Ernzerhof (PBE) was used for the electron exchange correlation potential[87]. Figure 8a shows the side and top views of the rhombohedral crystal structure of the 24 formula unit (f.u.) cell (120-atom) adopted for $Bi_{0.5}Na_{0.5}TiO_3$ (BNT). As model systems shown in Fig. 8b,c, we have considered the substitution of one Ba atom for the Bi-site, denoted as B(Ba)NT, and Na-site [BN(Ba)T], in the 24 f.u. cell structure of the BNT. This corresponds to about 0.83 at.% doping for the A-site (Bi and Na) substitution, which is within the range of the present experimental doping concentrations (0.5–9 mol.%). To represent the presence of the Fe substitution in a sample, we replaced one Ti [BNT(Fe)], Ba [B(Fe)NT], and Na [BN(Fe)T] atom with the Fe atom in the same unit cell, as shown in Fig. 9a–c. For all systems, we used an energy cutoff of 500 eV for the plane-wave basis and a *k*-point mesh of $5 \times 5 \times 5$ for the Brillouin

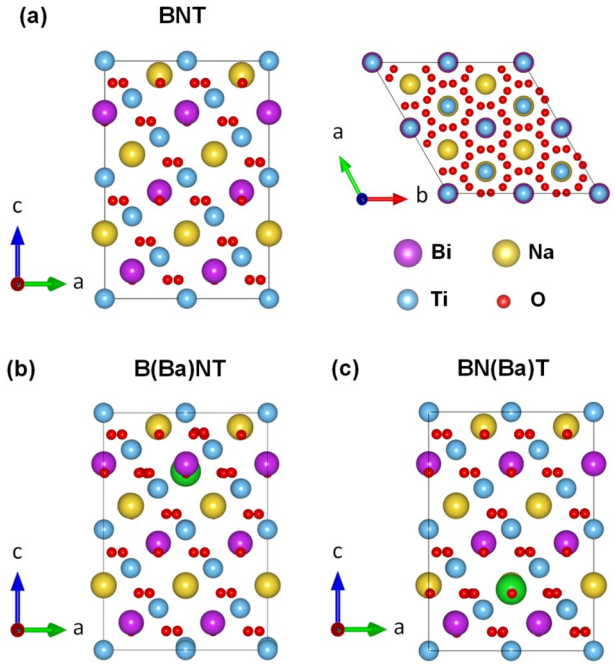

Figure 8. **(a)** Side and top views of the optimized atomic structure of $Na_{0.5}Bi_{0.5}TiO_3$ (BNT). The same with **(b)** Bi-site Ba [B(Ba)NT] and **(c)** Na-site Ba [BN(Ba)T] substitution.

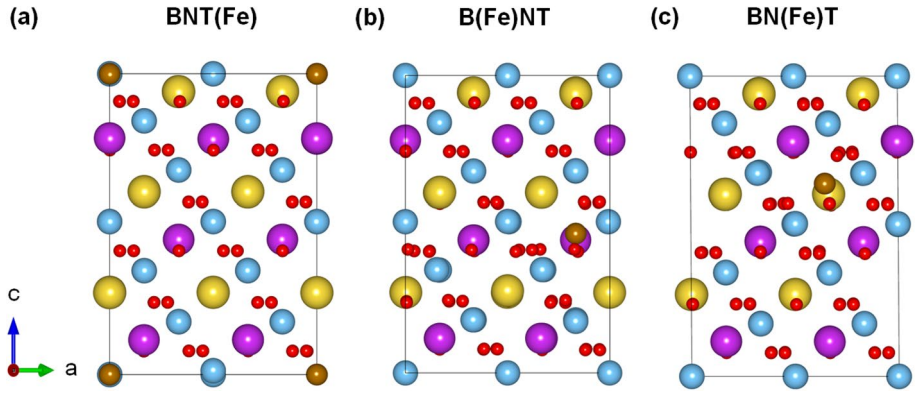

Figure 9. **(a)** Side views of the optimized atomic structure of the **(a)** Ti-site [BNT(Fe)], **(b)** Bi-site [B(Fe)NT], and **(c)** Na-site Fe [BN(Fe)T] substitution. The atomic symbols follow the same convention used in Fig. 8. Brown spheres are the Fe substitutional atoms.

zone integration. To obtain optimized atomic structures, the atomic positions as well as lattice parameters were fully relaxed until the largest force becomes less than 10^{-2} eV/Å and the change in the total energy between two ionic relaxation steps is smaller than 10^{-5} eV. Note that the severe distortions of octahedral TiO_3 lattice were observed for all geometries after optimization.

We first investigate the energetics of the Ba- and Fe-doped BNT. Here, the formation energy (H_f) is defined as $H_f = H - \sum_i \mu_i n_i$, where H is the total energy of the system, and μ_i and n_i are the chemical potential and the number of species i in the unit cell. The calculated H_f values of BNT, B(Ba)NT, BN(Ba)T, B(Fe)NT, BN(Fe)T, and BNT(Fe) are shown in Table 1. We find that the H_f of BNT is -2.385 eV/atom, which indicates the pure BNT is quite stable. Our calculations further indicate that the Ba substitute prefers either the Bi or Na sites (A-site), as their enthalpies of formation are competitive (− 2.402 and − 2.392 eV/atom). The Fe dopant atoms may also occupy both the A- and B-site (Ti), although the absolute values of H_f for the A-site (− 2.376 eV/atom for the Bi and − 2.355 eV/atom for the Na) are higher than that (− 2.335 eV/atom) of the B (Ti)-site in magnitude. Nevertheless, in a real sample, the latter substitution (B-site) might appear more than the A-site (Bi and Na) substitution, as the A-site is mainly occupied by the Ba atoms.

Table 1 shows the calculated magnetic energy ($\Delta E = E_{sp} - E_{non\text{-}sp}$, where E_{sp} and $E_{non\text{-}sp}$ are the total energies of the spin-polarized and non-spin-polarized states, respectively), total magnetization per f.u. (M), and atom

	H_f (eV/atom)	ΔE (eV)	M (μ_B/f.u.)	m (μ_B/atom)
BNT	−2.385	0	0	–
B(Ba)NT	−2.402	0	0	0
BN(Ba)T	−2.392	0	0	0
B(Fe)NT	−2.376	1.15	0.21	3.94
BN(Fe)T	−2.355	1.20	0.14	3.42
BNT(Fe)	−2.335	0.73	0.16	3.10

Table 1. The DFT results of the formation energy H_f (eV/atom), magnetic energy ΔE (eV/atom), and magnetization M (μ_B/f.u.) of BNT, B(Ba)NT, BN(Ba)T, B(Fe)NT, BN(Fe)T, and BNT(Fe) compounds. We also list the magnetic moment m (μ_B/atom) of the Fe dopant atom for the 1 Fe atom doped 24 f.u. cell of B(Fe)NT, BN(Fe), and BNT(Fe).

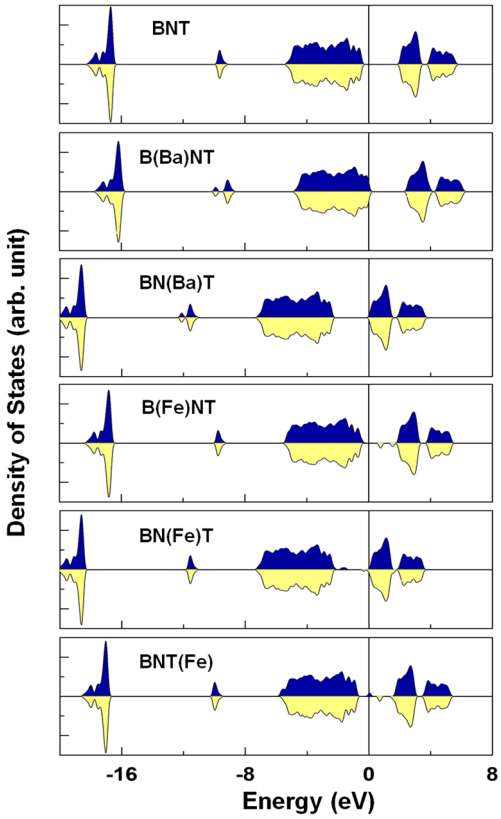

Figure 10. Top to bottom: The DFT results of the spin-resolved DOS for the BNT, B(Ba)NT, BN(Ba)T, BNT(Fe), B(Fe)NT, and BN(Fe)T. The Fermi level is set to zero energy.

resolved magnetic moment (m) of the dopant atoms. Our calculations show that all the Fe-doped structures are magnetic, while the Ba-doped ones are nonmagnetic. The calculated magnetization ranges from 0.14 to 0.21 μ_B/f.u. (or approximately 3.6 to 5.5 emu/g with [emu/g] = $1.078 \cdot 10^{20}$ ($M_{f.u.}/N_A$) [μ_B/f.u.], where the N_A and $M_{f.u.}$ are the Avogadro constant and the molar mass per f.u., respectively) at 0.83 at. % doping. These theoretical magnetization values are much higher than the maximum experimental value of 23 memu/g for 9 mol.% $BaFeO_{3-\delta}$-modified $Na_{0.5}Bi_{0.5}TiO_3$. The induced magnetization mainly comes from the local atomic moment of the Fe dopant atoms, as shown in Table 1.

Figure 10 presents the spin-resolved density of states (DOS) of BNT, B(Ba)NT, BN(Ba)T, B(Fe)NT, BN(Fe)T, and BNT(Fe) compounds. We have also analyzed the orbital projected DOS (PDOS) of the Fe 3*d* orbital states in Fig. 11 for the selected B(Fe)NT, BN(Fe)T, and BNT(Fe) as they exhibit magnetic nature. For BNT, the valence and conduction bands are characterized by the O-2*p* and Ti-3*d* orbital states with a band gap of ~ 2.25 eV, respectively. The majority- and minority-spin states are entirely degenerate, which indicates a feature of nonmagnetic ground state. The calculated band gap of BNT is smaller than the measured value (3.08 eV), which is quite typical in DFT calculations for oxide perovskites[88]. The Bi-site Ba gives rise to the upward shift of the valence band states toward the Fermi level. The opposite appears for BN(Ba)T, where the Fermi level shifts upward and touches the minimum of the conduction bands. Thus, the former and latter systems are referred to as *p*- and

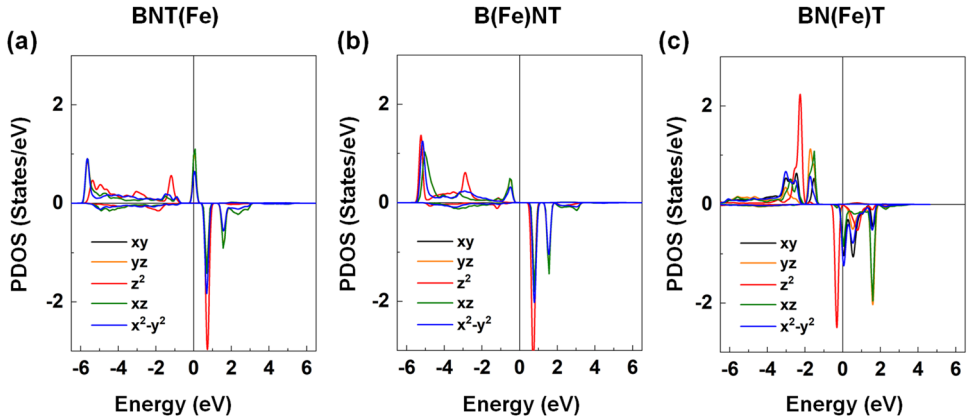

Figure 11. The DFT results of the *d*-orbital decomposed PDOS of the Fe substitutional atom for the **(a)** BNT(Fe), **(b)** B(Fe)NT, and **(c)** BN(Fe)T. The black, orange, red, green, and blue lines represent the d_{xy}, d_{yz}, d_{z^2}, d_{xz}, and $d_{x^2-y^2}$ orbital states, respectively. The Fermi level is set to zero energy.

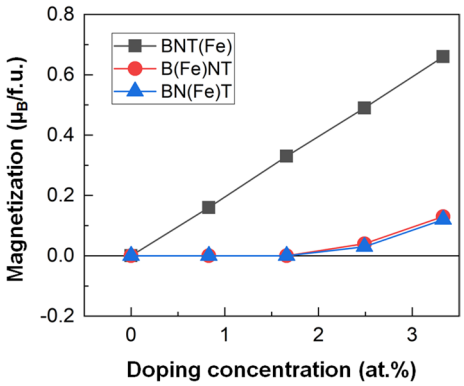

Figure 12. The DFT results of the magnetization (μ_B/f.u.) of BNT(Fe), B(Ba)NT, and BN(Ba)T as function of the concentration of the dopant atoms.

n-doped semiconductors, while kept the absolute value of the band gap. On the other hand, as shown in the bottom panels in Fig. 10, for B(Fe)NT, BN(Fe)T, and BNT(Fe), there are some midgap states around the Fermi level. In particular, for BNT(Fe), a finite DOS peak state appears right at the Fermi level in the majority-spin state while the other spin channel exhibits an insulating behavior. This is a feature of the half-metallic electronic nature. Furthermore, for all the Fe-doped compounds, substantially large exchange splitting between the spin subbands (i.e., majority-spin and minority-spin) is prominent (Fig. 10). These peak states are due to the strong orbital hybridization between the Fe 3*d* and O 2*p* states. As shown in Fig. 11, the majority-spin bands of the Fe are fully occupied, and the minority-spin states are almost unoccupied for the BNT(Fe) and B(Fe)NT but partially occupied for the BN(Fe)T. Overall, one can expect the large magnetic moment at the Fe site, as addressed in Table 1. Induced moments at the neighboring sites to the Fe are rather small.

Based on the PDOS analyses for the BNT(Fe) and B(Fe)NT compounds, we infer that the six (five) *d*-orbitals of Fe^{2+} (Fe^{3+}) ion split by high-spin state through the crystal field theory are filled by the 5 majority-spin electrons in the low-lying t_{2g} orbital levels and 1 electrons (no electron) in the minority-spin t_{2g} state. Thus, according to Hund's rule, the calculated magnetic moments of 4 and 5 μ_B of the Fe replacement for the Ti and Bi sites can be explained by the electronic configuration of the high-spin state in the crystal field theory through the unpaired electron spin count. For the BN(Fe)T, the magnetic moment of the Fe atom is reduced compared with those for the other two systems, as some minority-spin states are partially occupied (Fig. 11c). Furthermore, for all compounds, both the t_{2g} and e_g states in PDOS are slightly split, which is mainly due to the Jahn–Teller effect as the severe octahedron distortion occurs in the presence of the Fe substitution.

We now investigate the doping concentration dependent magnetization of the Fe and Ba doped BNT. Figure 12 shows the calculated *M* of BNT(Fe), B(Fe)NT, and BN(Fe)T as function of the concentration of the dopant atoms. For the 2 (or 1.67 at.%) and 4 (or 3.33 at.%) Fe atoms in the 24 f.u. cell, we have also considered the spin antiparallel coupling between the Fe dopant atoms. For both cases, the spin parallel coupling (ferromagnetic) is more preferable than the spin antiparallel coupling.

Clearly, the magnetization increases linearly from 0.16 μ_B/f.u. (4.2 emu/g) to 0.66 μ_B/f.u. (17.3 emu/g) as the Fe concentration increases from 0.83 at.% to 3.33 at.%, as shown in Fig. 12. Our calculated magnetization

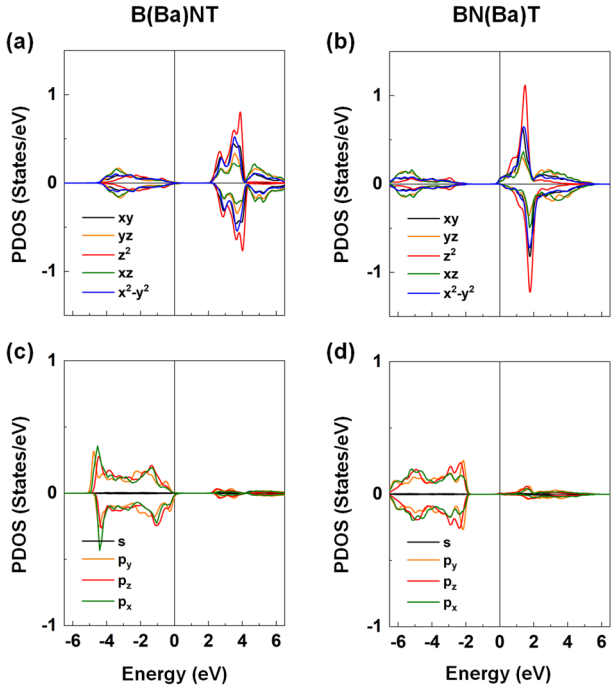

Figure 13. The DFT results of PDOS of the Ti and O atoms for **(a)** and **(c)** (Ba)NT and **(b)** and **(d)** BN(Ba)T at 3.33 at./% Ba doping. The Fermi level is set to zero energy.

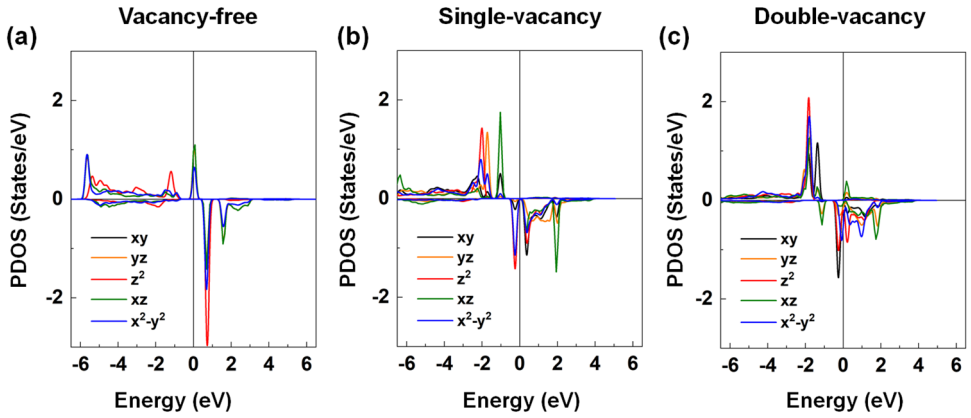

Figure 14. The DFT results of the *d*-orbital decomposed PDOS of the Fe substitutional atom for the BNT(Fe) with the **(a)** vacancy-free, **(b)** single-vacancy, and **(c)** double-vacancy. The black, orange, red, green, and blue lines represent the d_{xy}, d_{yz}, d_{z^2}, d_{xz}, and $d_{x^2-y^2}$ orbital states, respectively. The Fermi level is set to zero energy.

is much larger than the measured values (23 memu/g at 9 mol.%), which is presumably due to the different concentrations and stoichiometries between the theory (here only the Fe doping) and experiment (Ba and Fe co-doping). Interestingly, the Ba doping for the *A*-site (Bi and Na) induces magnetism ($M = 0.05\ \mu_B$/f.u.) at about 2.5 at.% (Fig. 12). It is further found that the calculated magnetization increases as the doping concentration increases. Our atom resolved magnetization analyses indicate that the induced magnetization mainly comes from the Ti and O atoms neighboring to the Ba dopant site. The underlying mechanism can be explained by the spin-polarized charge transfer between the dopant and neighboring atoms in the unit cell, as revealed from the Ti- and O-PDOS analyses shown in Fig. 13.

We finally explored the magnetic and electronic properties of the O-vacancy defected BNT(Fe). We have considered the presence of a single vacancy and double vacancies in the Fe-included octahedral cell to imitate different valence states of the Fe dopant atom. Our calculations show that the total magnetization (4 μ_B) of the BNT(Fe) compound decreases by 1 and 2 μ_B for the single-vacancy and double-vacancy systems, respectively. From the electronic structure analyses shown in Fig. 14a–c, the PDOS of the Fe dopant atom in BNT(Fe) shift toward the low energy region and some minority-spin states are partially occupied in the presences of the single and double oxygen vacancies. This is because of the extra electrons accumulated at the Fe site, originated from

the O deficiency in the unit cell. Furthermore, the obtained magnetic moments are simply the reflections of the Fe^{2+} and Fe^{3+} ionic states in the high spin states and mixture of them in a real sample, as addressed in the previous experiment[30].

Conclusion

The solid solution of $BaFeO_{3-\delta}$ and $Na_{0.5}Bi_{0.5}TiO_3$ ceramics have been successfully synthesized by a chemical route sol–gel method. The Ba and Fe ions were distributed randomly into the $Na_{0.5}Bi_{0.5}TiO_3$ lattices which caused in the distortion of lattice structure and decreased the optical band gap. The complex magnetic properties were observed in this solid solution. This work shows a simple way for enhancement of room-temperature ferromagnetism in lead-free ferroelectric materials by solid solution.

Experiment

$(1-x)Na_{0.5}Bi_{0.5}TiO_3 + xBaFeO_{3-\delta}$ (BNT-xBFO; $x = 0.5\%$, 1%, 3%, 5%, 7% and 9%) samples were fabricated by sol–gel method. The raw materials were consisted of $Bi(NO_3)_3{\cdot}5H_2O$, $NaNO_3$, $Fe(NO_3)_3{\cdot}9H_2O$, tetraisopropoxytitanium (IV) ($C_{12}H_{28}O_4Ti$) and $BaCO_3$. The solution was chosen which are acetic acid (CH_3COOH) and deionized water with volume ratio of V_{H_2O}:V_{CH_3COOH} = 5:2 while an acetylacetone ($CH_3COCH_2COCH_3$) were selected as ligand. Fist, the $BaCO_3$ were weighted and distinguee under mix acid acetic and deionized water. Thus, the raw materials such $Bi(NO_3)_3.5H_2O$, $NaNO_3$, $Fe(NO_3)_3.9H_2O$ were weighted to add the solution. To following, the solution was added with tetraisopropoxytitanium after adding to avoid hydrolysis. The solution was magnetic stirred under several hours to make homogeneous solution of sol. The sol was dried under 100 °C to prepare gels in oval. The dried gel was rout grounded and annealed under 800 °C for three hours in air then nature cooling down to room temperature. The as-prepared samples were rout ground for further samples characterization.

The chemical composition and chemical mapping of samples was carried out via energy dispersive spectroscopy (EDS, S-4800 Hitachi). The sodium is lighter element which were easy evaporated during the gelling and annealing processing that make samples nonstoichiometric composition. Therefore, the sodium nitrate was weighed to extra around 40–50 mol% to prevent the sodium evaporation[9–11,24–42,60]. The crystalline structural of pure $Na_{0.5}Bi_{0.5}TiO_3$ and $BaFeO_{3-\delta}$-modified $Na_{0.5}Bi_{0.5}TiO_3$ samples were characterized through X-ray diffraction (XRD, Brucker D8 Advance). The vibration modes of samples were measured by using Raman spectroscopy (with a 475 nm LASOS laser and a DU420A-Oe detector). The optical properties were studied by Ultraviolet–Visible (UV–Vis, Jasco V-670) and photoluminescence (PL, excited with 475 nm LASOS laser and a DU420A-Oe CCD detector) spectroscopy. Magnetic properties were characterized by a vibrating sample magnetometer (VSM, Lakeshore 7404). All experimental were performed at room temperature.

Received: 29 August 2020; Accepted: 1 April 2021
Published online: 26 April 2021

References

1. Eerenstein, W., Mathur, N. D. & Scott, J. F. Multiferroic and magnetoelectric materials. *Nature* **442**, 759. https://doi.org/10.1038/nature05023 (2006).
2. Hu, J. M., Nan, T., Sun, N. X. & Chen, L. Q. Multiferroic magnetoelectric nanostructures for novel device applications. *MRS Bull.* **40**, 728. https://doi.org/10.1557/mrs.2015.195 (2015).
3. N. D. Quan, L. H. Bac, D. V. Thiet, V. N. Hung, & Dung, D. D. Current development in lead-free $Bi_{0.5}(Na,K)_{0.5}TiO_3$-based piezoelectric materials. *Adv. Mater. Sci. Eng.* **2014**, 1–13, https://doi.org/10.1155/2014/365391 (2014).
4. Jo, W. *et al.* Giant electric-field-induced strains in lead-free ceramics for actuator applications – Status and perspective. *J. Electroceram.* **29**, 71. https://doi.org/10.1007/s10832-012-9742-3 (2012).
5. Rodel, J. *et al.* Transferring lead-free piezoelectric ceramics into application. *J. European Ceram. Soc.* **35**, 1659. https://doi.org/10.1016/j.jeurceramsoc.2014.12.013 (2015).
6. Baettig, P., Schelle, C. F., Lesar, R., Waghmare, U. V. & Spaldin, N. A. Theoretical prediction of new high-performance lead-free piezoelectrics. *Chem. Mater.* **17**, 1376. https://doi.org/10.1021/cm0480418 (2005).
7. He, X. & Jin, K. J. Persistence of polar distortion with electron doping in lone-pair driven ferroelectrics. *Phys. Rev. B* **94**, 224107. https://doi.org/10.1103/PhysRevB.94.224107 (2016).
8. Wang, Y., Xu, G., Ji, X., Ren, Z., Weng, W., Du, P., Shen, G., & Han, G. Room-temperature ferromagnetism of Co-doped $Na_{0.5}Bi_{0.5}TiO_3$: Diluted magnetic ferroelectrics. *J. Alloy Compound.* **475**, L25–L27. https://doi.org/https://doi.org/10.1016/j.jallcom.2008.07.073 (2009).
9. Dung, D. D. *et al.* Tunable magnetism of $Na_{0.5}Bi_{0.5}TiO_3$ materials via Fe defects. *J. Supercond. Novel Magn.* **32**, 3011. https://doi.org/10.1007/s10948-019-05163-z (2019).
10. Thanh, L. T. H. *et al.* Making room-temperature ferromagnetism in lead-free ferroelectric $Bi_{0.5}Na_{0.5}TiO_3$ material. *Mater. Lett.* **186**, 239–242. https://doi.org/10.1016/j.matlet.2016.09.105 (2017).
11. Thanh, L. T. H. *et al.* Origin of room temperature ferromagnetism in Cr-doped lead-free ferroelectric $Bi_{0.5}Na_{0.5}TiO_3$ materials. *J. Electron. Mater.* **46**, 3367. https://doi.org/10.1007/s11664-016-5248-0 (2017).
12. Zheng, G. P., Uddin, S., Zheng, X. & Yan, J. Structural and electrocaloric properties of multiferroic-$BiFeO_3$ doped $0.94Bi_{0.5}Na_{0.5}TiO_3$–$0.06BaTiO_3$ solid solutions. *J. Alloys Compound.* **663**, 294. https://doi.org/10.1016/j.jallcom.2015.12.056 (2016).
13. Kumar, Y. & Yadav, K. L. Dielectric, magnetic and electrical properties of $Bi_{0.5}Na_{0.5}TiO_3$ – $CoMn_{0.2}Fe_{18}O_4$ composites. *AIP Conf. Proc.* **1731**, 050090. https://doi.org/10.1063/1.4947744 (2016).
14. Ju, L., Xu, T. S., Zhang, Y. J. & Sun, L. First-principles study of magnetism in transition metal doped $Na_{0.5}Bi_{0.5}TiO_3$ system. *Chinese J. Chem. Phys.* **29**, 462. https://doi.org/10.1063/1674-0068/29/cjcp1602023 (2016).
15. Zhang, Y., Hu, J., Gao, F., Liu, H. & Qin, H. Ab initio calculation for vacancy-induced magnetism in ferroelectric $Na_{0.5}Bi_{0.5}TiO_3$. *Comput. Theor. Chem.* **967**, 284. https://doi.org/10.1016/j.comptc.2011.04.030 (2011).
16. Ju, L. *et al.* Room-temperature magnetoelectric coupling in nanocrystalline $Na_{0.5}Bi_{0.5}TiO_3$. *J. Appl. Phys.* **116**, 083909. https://doi.org/10.1063/1.4893720 (2014).
17. Rahman, J. U. *et al.* Dielectric, ferroelectric and field-induced strain response of lead-free $BaZrO_3$-modified $Bi_{0.5}Na_{0.5}TiO_3$ ceramics. *Curr. Appl. Phys.* **14**, 331. https://doi.org/10.1016/j.cap.2013.12.009 (2014).

18. Yang, J. *et al.* Dielectric, ferroelectric and piezoelectric properties of $Bi_{0.5}Na_{0.5}TiO_3$–$(Ba_{0.7}Ca_{0.3})TiO_3$ ceramics at morphotropic phase boundary composition. *Mater. Sci. Eng. B* **176**, 260. https://doi.org/10.1016/j.mseb.2010.12.007 (2011).
19. Bai, W. *et al.* Phase evolution and correlation between tolerance factor and electromechanical properties in BNT-based ternary perovskite compounds with calculated end-member $Bi(Me_{0.5}Ti_{0.5})O_3$ (Me = Zn, Mg, Ni, Co). *Dalton Trans.* **45**, 14141. https://doi.org/10.1039/C6DT01788F (2016).
20. Zhou, C. R. & Liu, X. Y. Dielectric properties and relaxation of $Bi_{0.5}Na_{0.5}TiO_3$-$BaNb_2O_6$ lead-free ceramics. *Bull. Mater. Sci.* **30**, 575. https://doi.org/10.1007/s12034-007-0090-x (2007).
21. Kaswan, K. *et al.* Crystal structure refinement, enhanced magnetic and dielectric properties of $Na_{0.5}Bi_{0.5}TiO_3$ modified $Bi_{0.8}Ba_{0.2}FeO_3$ ceramics. *Ceram. Inter.* **43**, 4622–4629. https://doi.org/10.1016/j.ceramint.2016.12.128 (2017).
22. Pattanayak, R., Raut, S., Kuila, S., Chandrasekhar, M. & Panigrahi, S. Multiferroism of [$Na_{0.5}Bi_{0.5}TiO_3$-$BaFe_{12}O_{19}$] lead-free novel composite systems. *Mater. Lett.* **209**, 280–283. https://doi.org/10.1016/j.matlet.2017.08.023 (2017).
23. Singh, S., Kaur, A., Kaur, P. & Singh, L. An investigation on cubic and monoclinic phase coexistence in sol-gel derived $LaFeO_3$-$Na_{0.5}Bi_{0.5}TiO_3$ ceramics. *J. Alloys Compound.* **857**, 158284. https://doi.org/10.1016/j.jallcom.2020.158284 (2021).
24. Hue, M. M. *et al.* Magnetic properties of (1–x)$Bi_{0.5}Na_{0.5}TiO_3$ + x$MnTiO_3$ materials. *J. Magn. Magn. Mater.* **471**, 164. https://doi.org/10.1016/j.jmmm.2018.09.087 (2019).
25. Hue, M. M. *et al.* Tunable magnetic properties of $Bi_{0.5}Na_{0.5}TiO_3$ materials via solid solution of $NiTiO_3$. *Appl. Phys. A* **124**, 588. https://doi.org/10.1007/s00339-018-2002-x (2018).
26. Dung, D. D. *et al.* Enhancing room-temperature ferromagnetism in $Bi_{0.5}Na_{0.5}TiO_3$ via $FeTiO_3$ solid solution. *J. Electroceram.* **44**, 129–135. https://doi.org/10.1007/s10832-020-00203-w (2020).
27. Dung, D. D. *et al.* Experimental and theoretical studies on the room-temperature ferromagnetism in new (1–x) $Bi_{1/2}Na_{1/2}TiO_3$+x$CoTiO_3$ solid solution materials. *Vacuum* **179**, 109551. https://doi.org/10.1016/j.vacuum.2020.109551 (2020).
28. Hung, N. T. *et al.* Room-temperature ferromagnetism in Fe-based perovskite solid solution in lead-free ferroelectric $Bi_{0.5}Na_{0.5}TiO_3$ materials. *J. Magn. Magn. Mater.* **451**, 183. https://doi.org/10.1016/j.jmmm.2017.11.015 (2018).
29. Hung, N. T. *et al.* Structural, optical, and magnetic properties of $SrFeO_{3-\delta}$-modified $Bi_{0.5}Na_{0.5}TiO_3$ materials. *Phys. B* **531**, 75. https://doi.org/10.1016/j.physb.2017.12.021 (2018).
30. Hung, N. T. *et al.* Intrinsic and tunable ferromagnetism in $Bi_{0.5}Na_{0.5}TiO_3$ through $CaFeO_{3-\delta}$ modification. *Sci. Rep.* **10**, 6189. https://doi.org/10.1038/s41598-020-62889-w (2020).
31. Dung, D. D., Hung, N. T. & Odkhuu, D. Structure, optical and magnetic properties of new $Bi_{0.5}Na_{0.5}TiO_3$-$SrMnO_{3-\delta}$ solid solution materials. *Sci. Rep.* **9**, 18186. https://doi.org/10.1038/s41598-019-54172-4 (2019).
32. Dung, D. D., Hung, N. T. & Odkhuu, D. Magnetic and optical properties of new (1–x)$Bi_{0.5}Na_{0.5}TiO_3$+x$CaMnO_{3-\delta}$ solid solution materials. *Mater. Sci. Eng. B* **263**, 114902. https://doi.org/10.1016/j.mseb.2020.114902 (2021).
33. Dang, D. D., Hung, N. T. & Odkhuu, D. Magnetic and optical properties of new (1–x)$Bi_{0.5}Na_{0.5}TiO_3$+x$BaMnO_{3-\delta}$ solid solution materials. *Appl. Phys. A* **125**, 465. https://doi.org/10.1007/s00339-019-2571-3 (2019).
34. Dung, D. D., Hung, N. T. & Odkhuu, D. Magnetic and optical properties of $MgMnO_{3-\delta}$-modified $Bi_{0.5}Na_{0.5}TiO_3$ materials. *J. Magn. Magn. Mater.* **482**, 31–37. https://doi.org/10.1016/j.jmmm.2019.03.029 (2019).
35. Dung, D. D. & Hung, N. T. Magnetic properties of (1–x)$Bi_{0.5}Na_{0.5}TiO_3$+x$SrCoO_{3-\delta}$ solid-solution materials. *Appl. Phys. A* **126**, 240. https://doi.org/10.1007/s00339-020-3409-8 (2020).
36. Dung, D. D. & Hung, N. T. Structural, optical, and magnetic properties of the new (1–x)$Bi_{0.5}Na_{0.5}TiO_3$+x$MgCoO_{3-\delta}$ solid solution system. *J. Supercond. Novel Magn.* **33**, 1249–1256. https://doi.org/10.1007/s10948-020-05451-z (2020).
37. Dung, D. D. & Hung, N. T. Structural, optical and magnetic properties of (1–x)$Bi_{0.5}Na_{0.5}TiO_3$+x$BaCoO_{3-\delta}$ solid solution systems prepared by the sol-gel method. *J. Nanosci. Nanotech.* **21**, 2604–2612. https://doi.org/10.1166/jnn.2021.19090 (2021).
38. D. D. Dung, and N. T. Hung. Magnetic properties of (1-x)$Bi_{0.5}Na_{0.5}TiO_3$+x$CaCoO_{3-\delta}$ solid-solution system. J. Electron. Mater. **49**, 5317–5325 (2020). https://doi.org/https://doi.org/10.1007/s11664-020-08233-4.
39. Dung, D. D. *et al.* Design and characterization of a new (1–x)$Na_{1/2}Bi_{1/2}TiO_3$+x$Bi(Ti_{1/2}Fe_{1/2})O_3$ solid solution. *Vacuum* **183**, 109815. https://doi.org/10.1016/j.vacuum.2020.109815 (2021).
40. Phuong, L. T. K. *et al.* Structural, optical, and magnetic properties of a new system $Bi(Mn_{0.5}Ti_{0.5})O_3$-modified $Bi_{0.5}Na_{0.5}TiO_3$ materials. *Mater. Res. Exp.* **6**, 106112. https://doi.org/10.1088/2053-1591/ab3ce0 (2019).
41. Dung, D. D., Hue, M. M. & Bac, L. H. Growth and magnetic properties of new lead-free (1–x)$Bi_{1/2}Na_{1/2}TiO_3$+x$Bi(Ti_{1/2}Co_{1/2})O_3$ solid solution materials. *Appl. Phys. A* **126**, 533. https://doi.org/10.1007/s00339-020-03718-9 (2020).
42. Dung, D. D. *et al.* Influenced of $Bi(Ti_{1/2}Ni_{1/2})O_3$ concentration on the structural, optical and magnetic properties of lead-free $Bi_{1/2}Na_{1/2}TiO_3$ materials. *Vacuum* **177**, 109306. https://doi.org/10.1016/j.vacuum.2020.109306 (2020).
43. Hong, N. H. *et al.* Shaping the magnetic properties of $BaFeO_3$ perovskite-type by alkaline-earth doping. *J. Phys. Chem. C* **122**, 2983. https://doi.org/10.1021/acs.jpcc.7b10127 (2018).
44. Suga, Y., Hibino, M., Kuno, T. & Mizuno, N. Electrochemical oxidation of $BaFeO_{2.5}$ to $BaFeO_3$. *Electrochim. Acta* **137**, 359. https://doi.org/10.1016/j.electacta.2014.05.162 (2014).
45. Mori, S. Phase transformation in barium orthoferrate, $BaFeO_{3-x}$. *J. Am. Ceram. Soc.* **49**, 600. https://doi.org/10.1111/j.1151-2916.1966.tb13176.x (1966).
46. Hayashi, N. *et al.* $BaFeO_3$: A ferromagnetic iron oxide. *Angew. Chem. Int. Ed.* **50**, 12547. https://doi.org/10.1002/anie.201105276 (2011).
47. Clemens, O. *et al.* Crystallographic and magnetic structure of the perovskite-type compound $BaFeO_{2.5}$: Unrivaled complexity in oxygen vacancy ordering. *Inorg. Chem.* **53**, 5911. https://doi.org/10.1021/ic402988y (2014).
48. Delattre, J. L., Stacy, A. M. & Siegrist, T. Structure of ten-layer orthorhombic $Ba_5Fe_5O_{14}$ ($BaFeO_{2.8}$) determined from single crystal X-ray diffraction. *J. Solid State Chem.* **177**, 928. https://doi.org/10.1016/j.jssc.2003.09.032 (2004).
49. Ju, S. & Cai, T. Y. Magnetic and optical anomalies in infinite-layer iron oxide $CaFeO_2$ and $BaFeO_2$: A density functional theory investigation. *J. Appl. Phys.* **106**, 093903. https://doi.org/10.1063/1.3238271 (2009).
50. Callender, C., Norton, D. P., Das, R., Hebard, A. F. & Budai, J. D. Ferromagnetism in pseudocubic $BaFeO_3$ epitaxial films. *Appl. Phys. Lett.* **92**, 012514. https://doi.org/10.1063/1.2832768 (2008).
51. Shannon, R. D. & Prewitt, C. T. Effective ionic radii in oxides and fluorides. *Acta Cryst. B* **25**, 925. https://doi.org/10.1107/S0567740869003220 (1969).
52. Chatzichristodoulou, C., Norby, P., Hendriksen, P. V. & Mogensen, M. B. Size of oxide vacancies in fluorite and perovskite structured oxides. *J. Electroceram.* **34**, 100. https://doi.org/10.1007/s10832-014-9916-2 (2015).
53. Niranjan, M. K., Karthik, T., Asthana, S. & Pan, J. Theoretical and experimental investigation of Raman modes, ferroelectric and dielectric properties of relaxor $Na_{0.5}Bi_{0.5}TiO_3$. *J. Appl. Phys.* **113**, 194106. https://doi.org/10.1063/1.4804940 (2013).
54. Chen, Y. *et al.* Structural and electrical properties of Mn-doped $Na_{0.5}Bi_{0.5}TiO_3$ lead-free single crystal. *Int. Ferroelectric* **141**, 120. https://doi.org/10.1080/10584587.2013.780141 (2013).
55. Thanh, L. T. H., Tuan, N. H., Bac, L. H., Dung, D. D., Bao, P. Q.. Influence of fabrication condition on the microstructural and optical properties of lead-free ferroelectric $Bi_{0.5}Na_{0.5}TiO_3$ materials. *Commun. Phys.* **26**, 51, https://doi.org/10.15625/0868-3166/26/1/7354 (2016).
56. Bac, L. H. *et al.* Tailoring the structural, optical properties and photocatalytic behavior of ferroelectric $Bi_{0.5}K_{0.5}TiO_3$ nanopowders. *Mater. Lett.* **164**, 631. https://doi.org/10.1016/j.matlet.2015.11.086 (2016).

57. Dung, D. D. *et al.* Room-temperature ferromagnetism in Fe-doped wide band gap ferroelectric $Bi_{0.5}K_{0.5}TiO_3$ nanocrystals. *Mater. Lett.* **156**, 129. https://doi.org/10.1016/j.matlet.2015.05.010 (2015).
58. Quan, N. D., Hung, V. N., Quyet, N. V., Chung, H. V. & Dung, D. D. Band gap modification and ferroelectric properties of $Bi_{0.5}(Na, K)_{0.5}TiO_3$-based by Li substitution. *AIP Adv.* **4**, 017122. https://doi.org/10.1063/1.4863092 (2014).
59. Tuan, N. H. *et al.* Defect induced room temperature ferromagnetism in lead-free ferroelectric $Bi_{0.5}K_{0.5}TiO_3$ materials. *Phys. B* **532**, 108. https://doi.org/10.1016/j.physb.2017.04.02560 (2018).
60. Dung, D. D. *et al.* Defect-mediated room temperature ferromagnetism in lead-free ferroelectric $Na_{0.5}Bi_{0.5}TiO_3$ materials. *J. Supercond. Novel Magn.* **33**, 911–920. https://doi.org/10.1007/s10948-019-05399-9 (2020).
61. Meng, J., Rai, B. K., Katiyar, R. S. & Zou, G. T. Study of visible emission and phase transition in nanocrystalline $A_{1-x}A'_xTiO_3$ systems. *Phys. Lett. A* **229**, 254. https://doi.org/10.1016/S0375-9601(97)00152-7 (1997).
62. Leite, E. R. *et al.* Amorphous lead titanate: a new wide-band gap semiconductor with photoluminescence at room temperature. *Adv. Funct. Mater.* **10**, 235. https://doi.org/10.1002/1099-0712(200011/12)10:6%3c235::AID-AMO409%3e3.0.CO;2-6 (2000).
63. Lin, Y. *et al.* Photoluminescence of nanosized $Na_{0.5}Bi_{0.5}TiO_3$ synthesized by a sol–gel process. *Mater. Lett.* **58**, 829. https://doi.org/10.1016/j.matlet.2003.07.025 (2004).
64. Dung, D. D. *et al.* Role of Co dopants on the structural, optical and magnetic properties of lead-free ferroelectric $Na_{0.5}Bi_{0.5}TiO_3$ materials. *J. Sci. Adv. Mater. Dev.* **4**, 584–590. https://doi.org/10.1016/j.jsamd.2019.08.007 (2019).
65. Shah, J. & Kotnala, R. K. Induced magnetism and magnetoelectric coupling in ferroelectric $BaTiO_3$ by Cr-doping synthesized by a facile chemical route. *J. Mater. Chem. A* **1**, 8601–8608. https://doi.org/10.1039/C3TA11845B (2013).
66. Cuong, L. V. *et al.* Observation of room-temperature ferromagnetism in Co-doped $Bi_{0.5}K_{0.5}TiO_3$ materials. *Appl. Phys. A* **123**, 563. https://doi.org/10.1007/s00339-017-1173-1 (2017).
67. Ren, Z. *et al.* Room-temperature ferromagnetism in Fe-doped $PbTiO_3$ nanocrystals. *Appl. Phys. Lett.* **91**, 063106. https://doi.org/10.1063/1.2766839 (2007).
68. Oanh, L. M., Do, D. B., Phu, N. D., Mai, N. T. P. & Minh, N. V. Influence of Mn doping on the structure, optical, and magnetic properties of $PbTiO_3$ material. *IEEE Trans. Magn.* **50**, 2502004. https://doi.org/10.1109/TMAG.2013.2297516 (2014).
69. Coey, J. M. D., Douvalis, A. P., Fitzgerald, C. B. & Venkatesan, M. Ferromagnetism in Fe-doped SnO_2 thin films. *Appl. Phys. Lett.* **84**, 1332. https://doi.org/10.1063/1.1650041 (2004).
70. Tuan, N. H., Linh, N. H., Odkhuu, D., Trung, N. N. & Dung, D. D. Microstructural, optical, and magnetic properties of $BiCoO_3$-modified $Bi_{0.5}K_{0.5}TiO_3$. *J. Electron. Mater.* **47**, 3414–3420. https://doi.org/10.1007/s11664-018-6166-0 (2018).
71. Tuan, N. H. *et al.* Structural, optical, and magnetic properties of lead-free ferroelectric $Bi_{0.5}K_{0.5}TiO_3$ solid solution with $BiFeO_3$ materials. *J. Electron. Mater.* **46**, 3472–3478. https://doi.org/10.1007/s11664-017-5328-9 (2017).
72. Durst, A. C., Bhatt, R. N. & Wolff, P. A. Bound magnetic polaron interactions in insulating doped diluted magnetic semiconductors. *Phys. Rev. B* **65**, 235205. https://doi.org/10.1103/PhysRevB.65.235205 (2002).
73. Coey, J. M. D., Venkatesan, M. & Fitzgerald, C. B. Donor impurity band exchange in dilute ferromagnetic oxides. *Nat. Mater.* **4**, 173–179. https://doi.org/10.1038/nmat1310 (2005).
74. Qiao, Y. *et al.* Local order and oxygen ion conduction induced high-temperature colossal permittivity in lead-free $Bi_{0.5}Na_{0.5}TiO_3$-based systems. *ACS Appl. Energy Mater.* **1**, 956–962. https://doi.org/10.1021/acsaem.7b00347 (2018).
75. Liu, X., Fan, H., Shi, J., Wang, L. & Du, H. Enhanced ionic conductivity of Ag addition in acceptor-doped $Bi_{0.5}Na_{0.5}TiO_3$ ferroelectric. *RSC Adv.* **6**, 30623–30627. https://doi.org/10.1039/C6RA00682E (2016).
76. Hejazi, M. M., Taghaddos, E. & Safari, A. Reduced leakage current and enhanced ferroelectric properties in Mn-doped $Bi_{0.5}Na_{0.5}TiO_3$-based thin films. *J. Mater. Sci.* **48**, 3511–3516. https://doi.org/10.1007/s10853-013-7144-9 (2013).
77. Dung, D. D., Thiet, D. V., Tuan, D. A. & Cho, S. Strain effects in epitaxial Mn_2O_3 thin film grown on MgO(100). *J. Appl. Phys.* **113**, 17A314. https://doi.org/10.1063/1.4794720 (2013).
78. Dung, D. D. *et al.* Strain modified/enhanced ferromagnetism in Mn_3Ge_2 thin films on GaAs(001) and GaSb(001). *J. Appl. Phys.* **113**, 153908. https://doi.org/10.1063/1.4802591 (2013).
79. Lan, Y. *et al.* Semiconducting tailoring and electrical properties of A-site Co substituted $Bi_{0.5}Na_{0.5}TiO_3$–δ ferroelectric ceramics. *Mater. Chem. Phys.* **260**, 124100. https://doi.org/10.1016/j.matchemphys.2020.124100 (2021).
80. Liu, L. *et al.* Ferroic properties of Fe-doped and Cu-doped $K_{0.45}Na_{0.49}Li_{0.06}NbO_3$ ceramics. *J. Mater. Sci. Mater. Electron.* **26**, 6592–6598. https://doi.org/10.1007/s10854-015-3257-z (2015).
81. Yang, A. M. *et al.* Copper doped $EuMnO_3$: synthesis, structure and magnetic properties. *RSC Adv.* **6**, 13982–13933. https://doi.org/10.1039/C5RA27426E (2016).
82. Deng, J. *et al.* Synthesis, structure and magnetic properties of $(Eu_{1-x}Mn_x)MnO_{3-\delta}$. *RSC. Adv.* **7**, 2019–2024. https://doi.org/10.1039/C6RA25951K (2017).
83. Deng, J. *et al.* The origin of multiple magnetic and dielectric anomalies of Mn-doped $DyMnO_3$ in low temperature region. *J. Alloys Comp.* **725**, 976–983. https://doi.org/10.1016/j.jallcom.2017.07.223 (2017).
84. Shannon, R. D. Revised effective ionic radii and systematic studies of interatomic distances in halides and chalcogenides. *Acta Cryst. A* **32**, 751–765. https://doi.org/10.1107/S0567739476001551 (1976).
85. Kresse, G. & Hafner, J. Ab initio molecular dynamics for liquid metals. *Phys. Rev. B* **47**, 558. https://doi.org/10.1103/PhysRevB.47.558 (1993).
86. Kresse, G. & Furthmuller, J. Efficient iterative schemes for *ab initio* total-energy calculations using a plane-wave basis set. *Phys. Rev. B* **54**, 11169. https://doi.org/10.1103/PhysRevB.54.11169 (1996).
87. Perdew, J. P., Burke, K. & Ernzerhof, M. Generalized gradient approximation made simple. *Phys. Rev. Lett.* **77**, 3865. https://doi.org/10.1103/PhysRevLett.77.3865 (1996).
88. Padilla, J. & Vanderbilt, D. *Ab initio* study of $BaTiO_3$ surfaces. *Phys. Rev. B* **56**, 1625. https://doi.org/10.1103/PhysRevB.56.1625 (1997).

Acknowledgements

This research is funded by The Ministry of Science and Technology, Viet Nam, under project number ĐTĐLCN.29/18. Prof. Yong Soo Kim thanks for the supporting from Priority Research Centers Program (2019R1A6A1A11053838), and the Basic Science Research Program (2021R1A2C1004209, 2020R1F1A1048657) through the National Research Foundation of Korea (NRF), funded by the Korean government. The research work at the Incheon National University was supported by Future Materials Discover Program (Grant No. 2016M3D1A1027831) and the Basic Research Program (Grant No. 2020R1F1A1067589) through the NRF grant funded by the Ministry of Science and ICT.

Author contributions

D.D.D. and N.H.L. conceived the idea and designed the experiments. N.H.L., N.A.D., N.N.T., N.V.D., and N.N.T. performed the experiments and measurements. D.O. performed the theoretical calculations and wrote

the corresponding paragraphs. D.D.D. and N.T.H. wrote the paper. Y.S.K. and A.D.N. reviewed and commented on the paper. All authors discussed the results and commented on the manuscript.

Competing interests
The authors declare no competing interests.

Additional information
Correspondence and requests for materials should be addressed to D.D.D., N.D., Y.S.K. or D.O.

Reprints and permissions information is available at www.nature.com/reprints.

Publisher's note Springer Nature remains neutral with regard to jurisdictional claims in published maps and institutional affiliations.